LANGMUIR

Interface Components: Nanoparticles, Colloids, Emulsions, Surfactants, Proteins, Polymers

The role of PEG-40-stearate in the production, morphology and stability of microbubbles

Joshua Owen, Sukanta Kamila, Shamit Shrivastava, Dario Carugo, Jorge Bernardino de la Serna, Christophoros Mannaris, Valerio Pereno, Richard Browning, Estelle Beguin, Anthony Patrick McHale, John F. Callan, and Eleanor Stride

Langmuir, **Just Accepted Manuscript** • DOI: 10.1021/acs.langmuir.8b02516 • Publication Date (Web): 28 Nov 2018

The role of PEG-40-stearate in the production, morphology and stability of microbubbles

J. Owen[1], S. Kamila[2], S. Shrivastava[1], D. Carugo[3], J. Bernadino de la Serna[4], C. Mannaris[1], V. Pereno[1], R. Browning[1], E. Beguin[1], A.P. McHale[2], J.F. Callan[2], E. Stride[1].

1. *Old Road Campus Research Building, University of Oxford, Oxford OX3 7DQ*

2. *School of Pharmacy and Pharmaceutical Science, University of Ulster, Coleraine. BT52 1SA*

3. Faculty of Engineering and the Environment, University of Southampton, Highfield, Southampton SO17 1BJ

4. Central Laser Facility, STFC Rutherford Appleton Laboratory, Harwell Campus, Didcot, OX11 0QX

ABSTRACT

Phospholipid coated microbubbles are currently in widespread clinical use as ultrasound contrast agents and under investigation for therapeutic applications. Previous studies have demonstrated the importance of the coating nanostructure in determining microbubble stability and its dependence upon both composition and processing method. Whilst the influence of different phospholipids has been widely investigated, the role of other constituents such as emulsifiers has received comparatively little attention. Herein, we present an examination of the impact of

polyethylene glycol (PEG) derivatives upon microbubble structure and properties. We present data using both pegylated phospholipids and a fluorescent PEG-40-stearate analogue synthesised in house to directly observe its distribution in the microbubble coating. We examine microbubbles of clinically relevant sizes, investigating both their surface properties and population size distribution and stability. Domain formation was only observed on the surface of larger microbubbles, which were found to contain a higher concentration of PEG-40-stearate. Lipid analogue dyes were also found to influence domain formation compared with PEG-40-stearate alone. "Squeezing out" of PEG-40-stearate was not observed from any of the microbubble sizes investigated. At the ambient temperature, microbubbles formulated with DSPE-PEG(2000) were found to be more stable than those containing PEG-40-stearate. At 37 °C, however the stability in serum was found to be the same for both formulations and no difference in acoustic backscatter was detected. This could potentially reduce the cost of PEGylated microbubbles and facilitate simpler attachment of targeting or therapeutic species. However, whether PEG-40-stearate sufficiently shields microbubbles to inhibit physiological clearance mechanisms still requires investigation.

INTRODUCTION

Ultrasound offers a safe, convenient and cost effective method of medical diagnostic imaging. Image contrast between blood vessels and the surrounding tissue, however, is typically lower than in other modalities such as Magnetic Resonance Imaging (MRI)[1]. To overcome this limitation, ultrasound contrast agents consisting of gas microbubbles stabilised by a surfactant or polymer coating[2] are injected into the patient's blood stream. Due to their high compressibility, microbubbles are able to scatter ultrasound much more efficiently than red blood cells. Moreover, they exhibit a non-linear response enabling the scattered signal to be distinguished from that due to neighbouring tissues [1]. Therapeutically, the oscillations of microbubbles under ultrasound can increase the permeability of both cell and tissue membranes for delivery of bioactive compounds [3]. Microbubbles are also being explored for use as oxygen carriers for the treatment of ischaemia and tumour hypoxia [4-6].

The key component of the microbubble for imparting stability and preventing coalescence is the coating. Microbubbles formulated with cross-linked serum albumin, such as Albunex® and Optison™ have relatively high coating stiffness and the propensity to rupture beyond a critical strain/expansion ratio, which limits the duration of contrast enhancement. To overcome this, Levovist® used a surfactant (palmitic acid) to provide a more flexible coating and hence improve the acoustic response but this resulted in a reduction in stability. Subsequently, however, it was found that other surfactants – such as phospholipids – could simultaneously provide stability and a strong acoustic response. This has led to multiple phospholipid formulations reaching the clinic, in particular Sonovue®

(Bracco Imaging), Sonazoid® (GE Healthcare) and Definity® (Bristol Myers-Squibb). In addition to phospholipids, smaller quantities of an emulsifier, typically polyethylene glycol are used in microbubble formulations to promote bubble formation, inhibit coalescence and reduce non-specific adsorption of blood plasma proteins[7].

Only a limited number of studies have been performed that examine the composition and structural properties of the phospholipid microbubble coating. For instance, Kim *et al.* analysed the mechanical properties of phospholipid monolayers using micropipette aspiration. They also employed fluorescent phospholipids and freeze fracture electron microscopy [8] to examine domain formation in the coating. This study utilised microbubbles composed of 10:1 lipid: PEG-40-stearate molar ratio and varied both lipid chain length and cooling time during bubble fabrication. The results indicated that the monolayer microstructure was dependent on the cooling rate with larger domains formed at slower cooling rates. Bubbles with a coarse domain structure exhibited a higher resistance to shear deformation than those with a fine structure.

Borden *et al.* examined the surface phase behaviour and microstructure of lipid/PEG-emulsifier coated microbubbles again with lipids of different chain length and a fluorescent dye (NBD-PC) *via* fluorescence microscopy and using lipid films in a Langmuir trough[9]. These results confirmed the polycrystalline nature of the two-component coating, and that the surface morphology was affected by the bubble fabrication process. NMR and FTIR spectroscopy were then employed to investigate lateral phase separation. These results indicated that, at

least in microbubbles greater than 10 μm in diameter, the coating comprised ordered domains consisting of lipid, and interdomain regions enriched by PEG-40-stearate[10]. It was also suggested that below a certain size (<20 μm) the bubble surface pressure would be too high for the emulsifier rich regions to co-exist with the lipid domains and would only remain attached through surface associated aggregates.

Lozano and Longo[11] employed fluorescence microscopy to study dissolving microbubbles coated with either a phosphatidylcholine (C16, C18 or C20) and PEG-40-stearate mixture or a phosphatidylcholine (C16, C18 or C20) and a PEG conjugated phospholipid (DSPE-PEG(2000)). Dissolution times for microbubbles containing DSPE-PEG(2000) were four times longer than those containing PEG-40-stearate. This is because the DSPE-PEG(2000) remains in the condensed phase with the lipid whereas with PEG-40-stearate it separates into the expanded phase, which is more gas permeable. Unlike the studies of Kim *et al*. and Borden *et al*., these experiments were performed with microbubbles in degassed water, using the lipid analogue DiIC18 fluorophore to examine domain formation and/or surface deformation. Moreover, these experiments were performed with air-filled bubbles (rather than the clinically used perfluorocarbons which have been shown to alter the properties of lipid membranes[12-14]) and at room temperature with bubbles of approximately 20 μm .

From these previous experiments the behaviour of the emulsifier was thus inferred from the observed lipid behaviour. Moreover, the fluorescence based

technique for the observation of lipid domains was applied on microbubbles above 5 μm only, to enable resolution of surface structures.

Kooiman *et al.* investigated the impact of lipid chain length on the distribution of ligands around the microbubble surface, using super-resolution microscopy. Two lipid chain lengths, DPPC (16 carbons) and DSPC (18 carbons), were used to make microbubbles with DSPE-PEG(2000)-biotin. Fluorescent streptavidin was attached to biotinylated microbubbles and a more even distribution and larger targeting area was found with DPPC relative to DSPC[15]. This was attributed to the fact that DSPE-PEG(2000)-biotin was more heterogeneously distributed on the microbubble surface in DSPC relative to DPPC, reducing the targeting area.

Abou-Saleh *et al.* examined the impact of PEGylated lipids on microbubbles created by microfluidics, and observed changes in microbubble stability and mechanical properties with increasing concentration of PEGylated lipid. Above a certain threshold, the lifetime and concentration of the microbubbles were seen to decrease[16]. Shih et al. performed similar experiments and found bubble lifetime to be related to stable size, and that bubble size reduced with increasing concentration of emulsifier, down to a threshold of 30% beyond which stability was compromised[17]. Segers *et al.* also found that during insonation shedding of the pegylated lipid from the microbubble can occur potentially altering the coating stiffness[18].

Recent results from Carugo *et al.* have shown transfer of material from the microbubble coating to nearby cell membranes and that polyethylene glycol has a major impact on lipid ordering and the extent of this lipid transfer[19]. Hosny *et al.* used molecular rotor fluorescence lifetime imaging in order to quantify the spatial distribution of viscosity in a microbubble coating. Varying composition and production methodologies indicated that there can be a large variation in viscosity across a microbubble population independent of the individual microbubble size [20].

The aim of this study is to build on the results of previous research examining the properties of microbubbles formulated with PEG-40-stearate. A fluorescent PEG-40-stearate analogue was synthesised to visualise the location of PEG-40-stearate in the microbubble coating. The impact of PEG-40-stearate concentration on the lipid packing was also examined via fluorescence spectral imaging of an environmentally sensitive fluorophore (c-laurdan). The concentration, size and stability of microbubbles formulated with both PEG-40-stearate and DSPE-PEG(2000) were then measured. Only one chain length of 18 carbons (DSPC) was used throughout the experiments for consistency. Finally the acoustic response of the difference microbubbles were compared.

MATERIALS AND METHODS

Materials

1,2-distearoyl-sn-glycero-3-phosphocholine (DSPC) was purchased from Avanti polar lipids Inc. (Alabaster, Alabama, USA). PEG-40-stearate, ethanol, chloroform, PEG (2000), stearoyl chloride and human serum were purchased from Sigma Aldrich Ltd. (Gillingham, Dorset, UK). C-laurdan was received as a kind gift from Dr Erdinc Sezgin (Weatherall Institute of Molecular Medicine, University of Oxford, Oxford, UK) but can be purchased from Stratech Scientific Ltd, Cambridge House, St Thomas' Pl, Ely). PEG (2000) FITC and Fluorescein-PEG-NH_2(MW=2000) were purchased from NANOCS (ChemQuest, Co., LTD, Springfield House, Water Lane, Wilmslow, Cheshire, SK9 5BG, UK). Dil Stain (1,1'-Dioctadecyl-3,3,3',3'-Tetramethylindocarbocyanine Perchlorate) was purchased from Thermo fisher Scientific Ltd, USA.

Microbubble and vesicle preparation

The relevant mixtures of lipids and emulsifier, dissolved in chloroform, were mixed in a glass vial at a selected molar ratio (9:1) lipid to emulsifier [9, 11, 20]. This was heated to 50 °C and left for 12 hours. The lipid film was suspended in aqueous solution (2 ml) for over 1 hour at 75 °C under constant stirring. The stir bar was removed, the solution was then sonicated for 90 s using an ultrasonic cell disruptor (XL2000, probe diameter 3 mm; Misonix Inc., Farmingdale, NY, USA) operating at 22.5 kHz and level 4 corresponding to 8 W_{RMS} output power. Sonication at the gas water interface in an SF_6 gas environment was then performed for 20 s, at sonication level 19 (38 W_{RMS}). The microbubble suspension

was then placed in an ice bath for cooling, for approximately 10 minutes. The same procedure was followed for vesicles but the last sonication step was omitted.

For those experiments involving fluorescent labelling of microbubbles, a stock solution of the lipophilic dye DiI at a concentration of 2.5 mg/mL in dimethyl sulfoxide (DMSO, Sigma Aldrich, UK) was prepared. 7 µL of the stock solution were added to the chloroform lipid solution, and the protocols outlined previously were followed for microbubble production. In order to remove excess DiI from the formed microbubble suspension, the microbubble sample was centrifuged once at 1000 g for 10 min (400R Heraeus Labofuge, Thermo Fisher Scientific Inc., USA), and microbubbles were re-suspended in PBS after each centrifugation cycle.

Synthesis of Fluorescein labelled PEG-40-Stearate

Fluorescein-PEG- Stearate was synthesized according to Scheme 1.

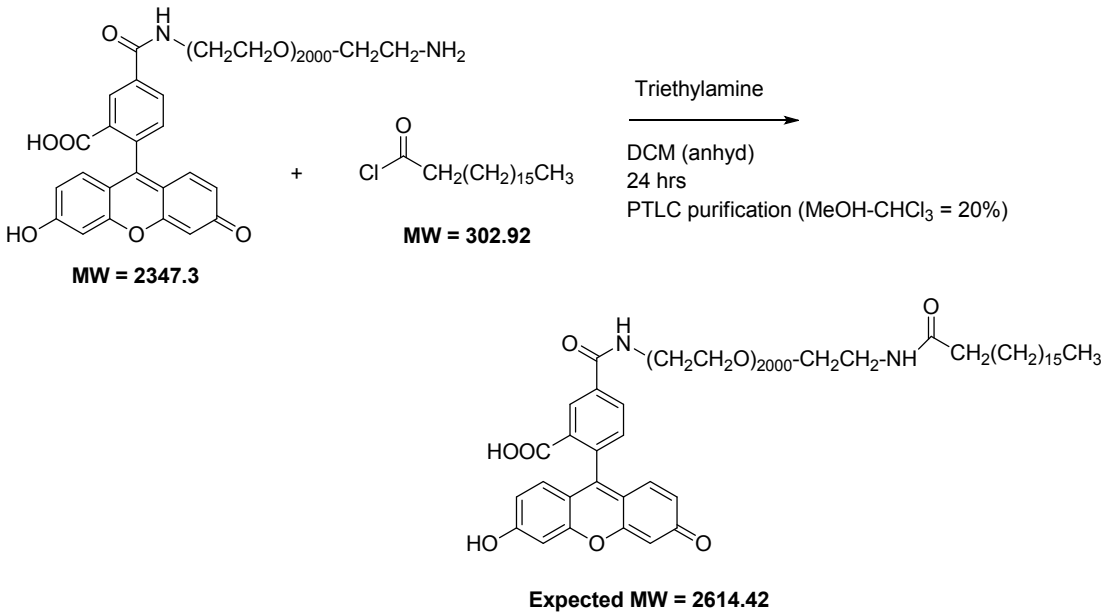

Scheme 1. Synthesis of Fluorescein-PEG- Stearate

To an ice cold solution (5 ^{o}C) of Fluorescein-PEG-NH_2 (50mg, 0.02 mmol) in anhydrous dichloromethane (5 ml) under N_2 atmosphere was added a catalytic amount of triethylamine. The solution was stirred for 30 mins at 5 ^{o}C and a solution of stearoyl chloride (7mg, 0.02 mmol) in anhydrous dichloromethane (5ml) was added dropwise maintaining the temperature between 0-5 ^{o}C. The reaction was allowed to proceed at room temperature for 24 hrs and kept in the dark. The product Fluorescein-PEG-Stearate was recovered by dissolution in dichloromethane and precipitation in ether, and finally purified by preparative thin layer chromatography using Methanol-Chloroform (20%) as the elutant.

Measurement of Lipid Order and lipid structure in the Microbubble coating

C-Laurdan staining

The lateral order of the lipids within the microbubble coating was quantified using C-Laurdan, an environmentally-sensitive fluorescent probe, the emissions from which shift according to the degree of hydration in the membrane. This technique has been widely used to characterise the surface properties of lipid structures, including investigation of the interactions between microbubbles and cells[19]. In order to reduce fluorescence background due to lipids in suspension, microbubbles were washed once by centrifugation. Approximately 3 mL of freshly prepared microbubbles were loaded into a disposable 10 mL Luer-Lok syringe (BD, MediSupplies, Unit 3, 2 Lansdowne Crescent, Bournemouth, UK) adapted to fit upright within a 50 mL centrifuge tube (Corning, Fogostraat 12, 1060 LJ Amsterdam, The Netherlands). They were then centrifuged at 1000g relative centrifugal force (RCF) at 10^{o}C for 10 minutes in a swing bucket rotor (Heraeus

Labofuge 400R, Thermo Fisher Scientific, 168 third avenue, Waltham, MA, USA) to form a bubble "cake" against the plunger. The subnatant was discarded and the bubbles resuspended within the syringe using 2 mL of PBS. This was then transferred to a glass vial for future use. To stain with C-Laurdan, 1.5 to 5 µL of C-Laurdan (400nM) was added to 30 µL of washed microbubbles diluted in 70 µL of Milli-Q water (total sample volume = 100 µL). This was incubated for up to 30 minutes at 4^{o}C before use.

Spectral fluorescence imaging

Spectral imaging was performed on a LSM 780 Inverted Confocal Microscope (Carl Zeiss Microscopy GmbH, Jena, Germany) using a previously reported methodology[21]. Briefly, 10 µL of stained microbubbles was loaded onto a 170 µm-thick glass slide coverslip (Logitech Ltd., Scotland) and covered with another coverslip. Individual microbubbles were then located and imaged using an oil immersed 63x objective, with the microscope focus set at the midplane of the microbubble. Spectral imaging was performed using a Zeiss LSM 780 confocal microscope (Carl Zeiss Microscopy GmbH, Jena, Germany), equipped with a 32-channel GaAsP detector array. C-Laurdan was excited at 405 nm, and the lambda detection range was set between 415 nm and 691 nm. This resulted in a single image stack, with each image providing the intensity map at a single emission wavelength (n=30). Approximately 20 images were taken per formulation, and each formulation was repeated three times using a freshly prepared microbubble suspension created from a new lipid film.

Generalised Polarisation (GP) calculation

Generalised polarization (GP) is an optical observable that quantifies the shift in the emission spectra of the dye. It provides an order parameter for the phase transition discussed above and is related to the dielectric properties of its microenvironment, which in turn directly affected by the presence of water in the lipid film. For example, an increase in hydration causes a red shift in the spectrum which corresponds to an increase in GP values. GP (ranging from -1 to +1) was utilised as a relative measure of lipid packing within the microbubble shell. To measure this, fluorescence microscopy images were processed using a custom script in MATLAB (The Mathworks Inc.). Briefly, images were first opened using the BioFormats for MATLAB script. Microbubbles were identified by a semi-automated implementation of the imfindcircles() function and the background and internal volume of the bubble removed by cropping, leaving only the pixels of the stained bubble coating [21]. This was done to reduce anisotropy effects and out-of-focal plane effects of the coating. GP values were calculated (per pixel) using intensity data from the 440 nm and 490 nm wavelength stacks by the following equation[22]:

1) $$GP = \frac{I_{440} - I_{490}}{I_{440} + I_{490}}$$

Increased GP value corresponds to an increase in the lipid order of the coating layer, and vice versa. Whole microbubble GP values were calculated from the average of the GP per pixel values. Standard deviations, medians and histogram plots were also generated from these data. Images with saturation (intensity of 255) in any wavelength were discarded. For spectral analysis, average intensity values of the coating per wavelength were calculated from pixel intensity values [20].

Lipid domain analysis by Langmuir Trough

Lipids from commercial stocks were used without further purification and were mixed in chloroform to obtain desired ratios at 25 mg/ml. 2 μl was then spread at the air-water interface in a Langmuir trough (microtrough G2, Kibron, Malminkaari, Helsinki, Finland) with an initial area of 212 cm^2. The trough was compressed at 50 cm^2/min and the pressure was recorded using a Wilhelmy plate at room temperature. Fluorescence images of the DSPC:PEG-40-Stearate monolayer were obtained by titrating the lipids under a microscope in 100 mm diameter petri dish. The amount of lipids to be titered was estimated from the isotherm on the Langmuir trough.

Fluorescence microscopy of microbubbles

The stained microbubbles were pipetted on to a 1.5H 75 x 25 mm glass slide and a cover slip was placed to prevent movement of the sample. A Zeiss LSM 780 confocal microscope equipped with a 63x Plan-Apochromat objective was used for imaging the microbubbles in the equatorial plane. The pinhole was adjusted to modify the thickness of the imaging plane and capture the phase separation on the microbubble surface. The imaging was performed on two separate channels: the first involved a 543 nm excitation and detectors set to a 553-673 nm range for detection of DiI; the second consisted of a 488 nm excitation with detectors set to acquire at 493-553 nm for detection of FITC. Intensity/pixel was determined using ImageJ public domain software (NIH, Bethesda, MD) by selecting the total area of the microbubble shell in midplane and measuring the raw intensity and the number of pixels.

Structure of Fluorescent PEG-40-stearate analogue

Mass Spectroscopy determination of molecular weight

Matrix Assisted Laser desorption/Ionisation – Time of flight (Maldi-TOF) spectra of Fluorescein-PEG-Stearate (Figure 1) was performed in Voyager-DM-Bio spectrometer using 50 µL of 1mg/3mL sample mixed with 100 µL of DHB matrix, where the laser intensity was 1471. The number average molecular weight (Mn) and average molecular weight (Mw) were calculated by the following equation:

2) $$M_n = \Sigma N_i M_i / \Sigma N_i$$

3) $$M_w = \Sigma N_i M_i^2 / \Sigma N_i M_i$$

Where M_i is the molecular weight of the chain and N_i is the number of chains of that molecular weight.

^{1}H NMR Spectra Determination of molecular structure

To determine the structure and confirm the synthesis had been successful the 1H NMR spectrum of Fluorescein-PEG-Stearate was recorded at room temperature using a Varian spectrometer operating at 500 MHz by using CDCl3 as solvent. The relative frequency of a nucleus relative to a standard in a magnetic field or Chemical shifts (δ) are given in parts per million (ppm) using tetramethylsilane (TMS) as an internal reference.

Microbubble Characterisation

Microbubble size and stability

Microbubble suspension (10 µl) was added to a Neubauer haemocytometer (Sigma Aldrich Ltd. Gillingham, Dorset, UK). This was then imaged using a Leica DM500 optical microscope (Larch House, Milton Keynes, MK14 6FG) and a 40 x

objective lens, at room temperature. In order to obtain a representative size distribution for one batch of bubbles; at least 3 separate bubble samples must have 30 images taken via optical microscopy[23]. The bubble size distribution and concentration were then determined using a purpose written image analysis software in Matlab (2013b, The Mathworks, Natick, MA, USA). The software converts each micrograph to a binary image and single spheroid shapes are then detected, measured and counted for each of the images analysed. A size distribution and count are then produced for the microbubbles. Since the dimensions of the haemocytometer and the microscope field of view are known, the volume concentration of microbubbles can also be estimated.

Nanoparticle size measurement

To determine the presence and size of vesicles, measurements of lipid dispersions before sonication at the gas/water interface were performed *via* dynamic light scattering using a Zetasizer Nano-ZS, Malvern Instruments Ltd. (Worcestershire, UK) in a disposable capillary cell (DTS1070 Malvern Instruments Ltd, Worcestershire, UK). Each sample of the liposome or microbubble solution (60 µl) was added to 940 µl of 10% HEPES buffer.

Microparticle size measurement

Laser light obscuration and scattering of microbubbles was used to obtain accurate size and concentration using an Accusizer 780, NICOMP Particle Sizing System (Santa Barbara, CA). 10 µl samples of each microbubble suspension were diluted into a 50 mL flask under mild mixing during measurement.

Microbubble stability in serum

DSPC microbubbles at 9:1 molar ratio with PEG-40-Stearate or DSPE-PEG-2000 and a set total concentration of 3mg/ml were created, kept on ice and added to serum. The microbubble size was then measured *via* the Accusizer. 10 µl of the microbubble suspension were added to 500 µl of serum giving a concentration of 10^7 microbubbles/ml. This is 10 x the blood concentration of microbubbles *in vivo* [24], but was used as lower concentrations could not be detected. The Accusizer was calibrated to remove the contribution of particles in the serum. The change in microbubble concentration was then measured over time for 15 minutes (the typical half-life of microbubbles in the in the human body being less than 5 minutes)[25]. This was performed at both room temperature and 37ºC.

Measurement of backscatter acoustic intensity of microbubbles

Imaging of the microbubbles and measurement of their response to ultrasound was carried out using a tissue-mimicking agarose flow phantom model with an embedded 1.2mm channel [26]. A peristaltic pump (Minipuls Evolution, Gilson Scientific UK, 3B Humphrys Road, Woodside Estate, Dunstable, Bedfordshire, LU5 4TP) was used to flow the freshly prepared microbubble solution (500µl) through the channel at a flow rate of 2 ml/min. An L12-5 probe of the iU-22 diagnostic ultrasound scanner (Philips Medical Systems, Bothell, WA) was used to interrogate and image the microbubbles at Contrast Mode and a low non-destructive Mechanical Index (MI=0.04). The frame rate was set at 1 Hz to ensure replenishment of the channel with fresh microbubbles and video loops of at least 10 images were captured. Quantification of the average backscatter intensity was done in Matlab (Mathworks, Natick MA, USA). The procedure was repeated for three separate solutions for each type of microbubble. Experiments were carried

out in a degassed water tank at 37 °C. Statistical analysis was performed using a 1 tailed student's t-test.

RESULTS AND DISCUSSION

Characterisation of fluorescein-PEG-stearate.

Successful formation of the fluorescein-PEG-stearate was confirmed by ^{1}H NMR spectroscopy with figure 1 showing the stacked spectra of the starting material fluorescein-PEG-NH_2 and the product fluorescein-PEG-stearate. Resonances in the downfield region (i.e. between 6.0 and 8.0) ppm were attributed to the aromatic protons of the fluorescein ring and were largely unchanged in the spectrum of the product given their distance from the site of conjugation. Examination of the upfield region, however, revealed the appearance of three new resonances in the spectrum of the product at 0.88, 1.40 and 2.10 ppm, that were not present in the spectrum of the starting material and represent the methyl protons, the protons from the 15 methylene groups of the stearic acid aliphatic chain and the methylene protons adjacent to newly formed amide carbonyl group, respectively. The broad peak at 3.9 ppm in both spectra was characteristic of methylene protons in the PEG polymer chain and again their chemical shift remained unchanged in the product when compared to the starting material. This was expected as their proximity to the newly created amide bond was separated by the two methylene groups minimising any change to their electronic environment following conjugation. The ratio of the integrals for the new methyl protons and the 8 aromatic protons was also consistent with successful product confirmation.

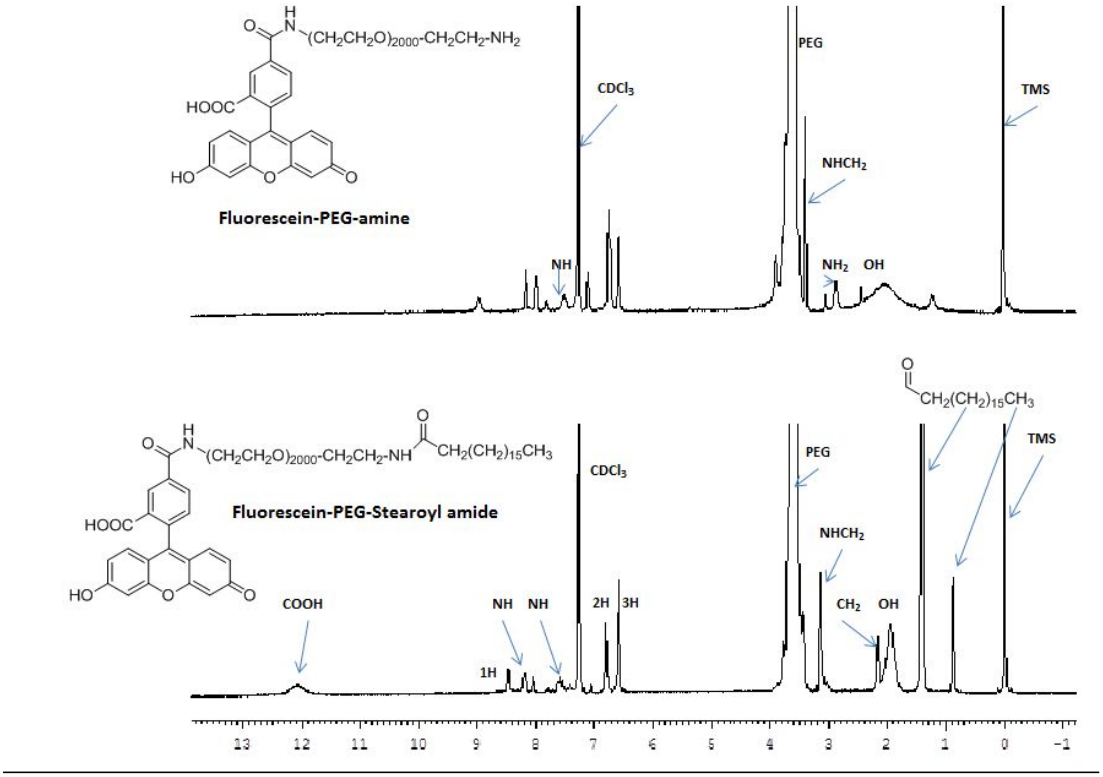

Figure 1, ^{1}H NMR spectra of Fluorescein-PEG and Fluorescein-PEG- Stearate (Solvent: $CDCl_3$).

The molecular weight of fluorescein-PEG-stearate was also analysed by MALDI-TOF mass spectroscopy (Figure 2). Given the polymeric nature of the PEG component of fluorescein-PEG-stearate, it is difficult to identify an exact molecular weight for this compound. However, assuming the total repeat unit weight was exactly 2000 Da, the MW would be expected to be 2614 Da. Similarly, the fluorescein-PEG-NH_2 precursor would be expected to have a MW = 2347 Da. Analysis of the MALDI-TOF spectrum revealed the Fluorescein-PEG-Stearate had a Mn and Mw of 2619 Da and 2654 Da respectively, with a polydispersity (Mw/Mn) of 1.01. While there is a sight discrepancy between the expected 2614 Da and observed 2619 Da, the observed MW range strongly suggests the successful formation of fluorescein-PEG-stearate with the small difference

attributed to variability in the PEG chain length. Combined, these analyses confirm the successful preparation of fluorescein-PEG-stearate.

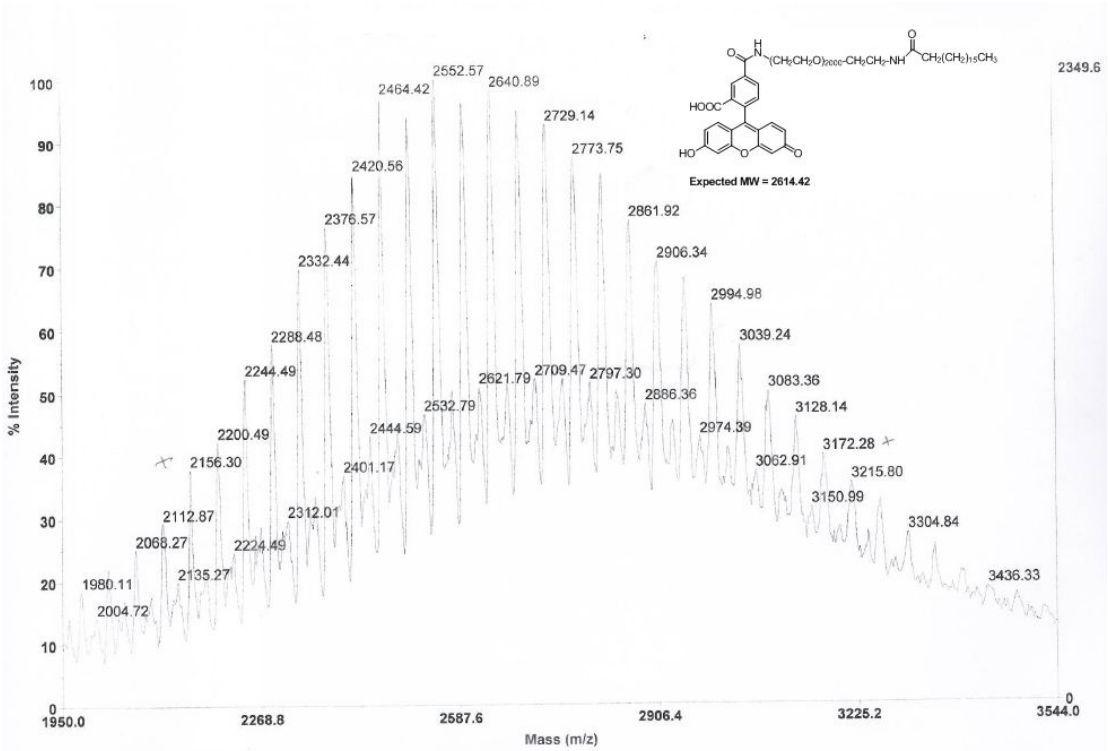

Figure 2, Maldi-TOF spectra of Fluorescein-PEG- Stearate amide indicating that stearic acid had been attached to the fluorescent PEG chain.

Langmuir trough analysis

Figure 3 characterizes the DSPC:PEG-40-Stearate (9:1) monolayer at the air water interface with the fluorescent PEG-40-stearate analogue, at 1% concentration of PEG-40-stearate. The lateral pressure vs area $(\pi - a)$ behaviour for several different lipid formulations containing DSPC lipids is shown in Figure 3A. The pure DSPC monolayer shows the well know sublimation (gas to liquid condensed) transition at 0mN/m where the pressure starts to rise abruptly[27]. The isothermal compressibility of the monolayer can be obtained from k_T (equation 4).

4) $$k_T = -\frac{1}{a}\left(\frac{\partial a}{\partial \pi}\right)_T$$

The data indicate that the DSPC monolayer is very stiff over the entire range (0 to 50 mN/m) of surface pressures. For DSPC:DSPE-PEG(2000) the compressibility is similar at high pressures, but the curve is shifted to the right. The DSPC, PEG-40-Stearate (9:1) monolayer on the other hand is qualitatively different from both DSPC alone and DSPC:DSPE-PEG(2000). A distinct region of low compressibility appears around 35mN/m. Such a plateau might be associated with a conformational transition in the components of lipid monolayers [11]. However, it would then be expected to show temperature, concentration and lipid chain length dependence [27]. Previous work has shown that this is not the case for monolayers containing PEG-40-Stearate [9] and instead that the plateau coincides with PEG-40-Stearate driven expulsion of material from the interface. The evidence of vesicular structures appearing in Figure 3 D supports this explanation.

Domain like features were observed at pressures as low as 10 mN/m and could be clearly resolved at 25mN/m. These domains continued to grow in size on further compression showing extensive phase separation at 40 mN/m with evidence of vesicles forming at the interface. These results are consistent with those of Lozano and Longo wherein PEG-40-stearate was found to create less stable microbubbles than DSPE-PEG(2000)[11]. These also concur with the results of Carugo *et al,* which indicated that PEG-40-stearate and lipids are able to leave the microbubble coating and pass into the surrounding liquid[19].

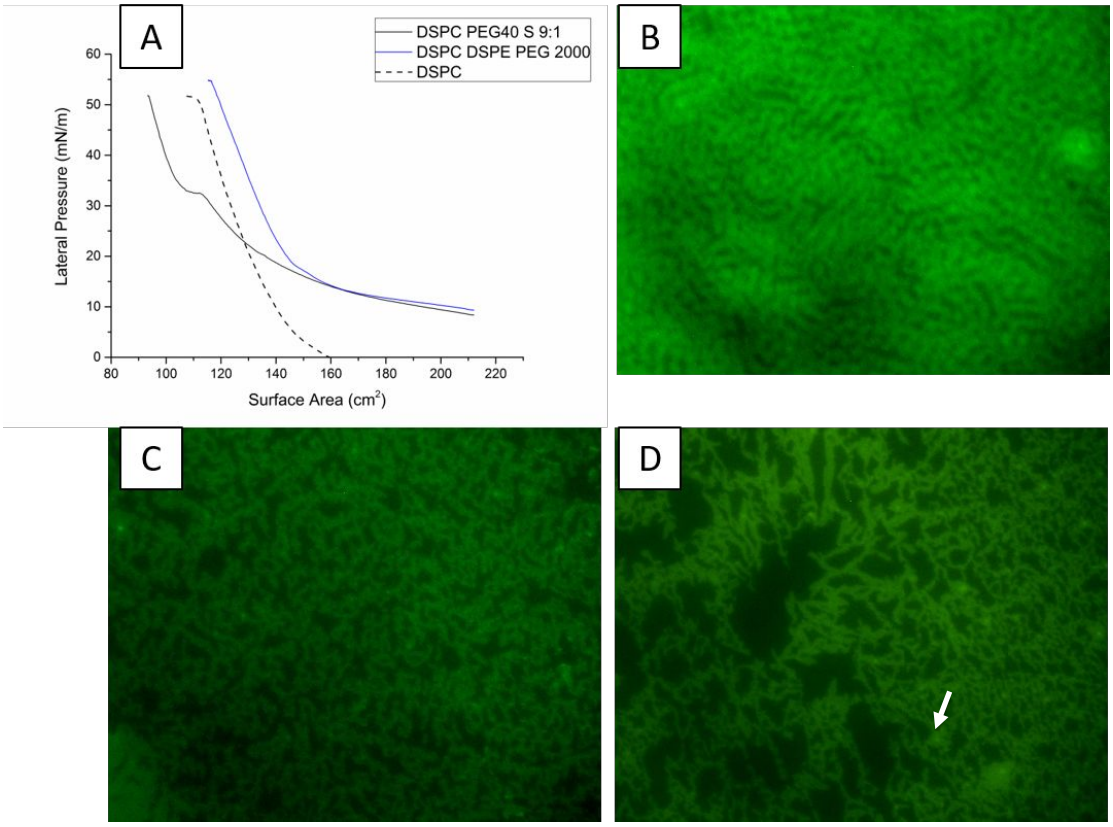

Figure 3, Langmuir trough measurements at A) Lateral pressure *vs* area isotherms of DSPC monolayer with and without modifications, B) low (~10mN/m), C) medium (~25mN/m) to D) high lateral pressure (~40mN/m) showing the formation of domains in a mixed film of fluorescent PEG-40-stearate analogue in DSPC. Arrow indicates vesicle like structures.

Impact on coating lipid order

The packing density of the lipids in the microbubble coating was analysed by calculating the Generalised Polarisation (GP) from spectral microscope images of C-Laurdan (Figure 4). GP values of microbubbles from spectral microscopy images were averaged and weighted to determine a mean GP for each formulation. Fluorescence microscopy images were also used to determine microbubble size and any relationship between mean GP and size. The GP values presented have

not been weighted by pixel number and values are pooled from all three repeats. Thus GP values for microbubbles below 2 μm may be more affected by noise as fewer pixels are used to calculate mean GP values.

For the range of bubble sizes investigated, increasing the concentration of PEG-40-stearate had no statistically significant effect upon the packing density of lipids in the microbubble coating. This agrees with the previous study of Hosny *et al.* which indicated that there was greater variability within a microbubble population than between microbubble populations [20]. It is also consistent with the suggestion in Borden *et al*. [10] that PEG-40-stearate is excluded from the coating when the microbubble diameter is smaller than 2 μm and thus no difference in properties would be observed.

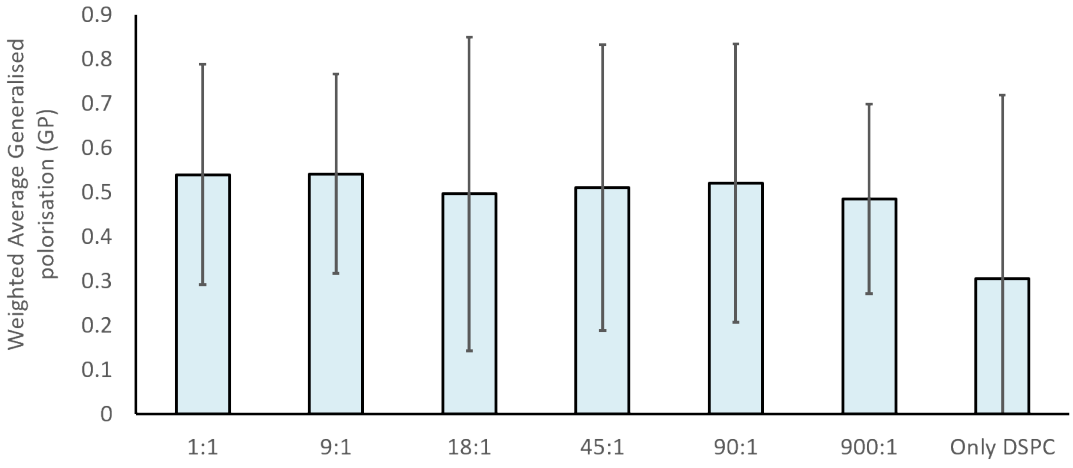

Figure 4, Weighted average generalised polarisation, at different ratios of DSPC to PEG-40-Stearate (n = 35)

Fluorescence microscopy images of Bubbles

Fluorescence Microscopy with FlTC-PEG-40-stearate and DiI

Images were taken of DSPC:PEG-40-stearate microbubbles that had been stained with DiI and contained 1% PEG-40-stearate-FITC (Figure 5). Intensity analysis of the confocal image stacks indicated that larger microbubbles (>20 μm) had a higher intensity per pixel at 5570 ± 141 AU/pixel than smaller microbubbles (<20 μm) at 2644 ± 193 AU/pixel when the midplane was examined. The opposite effect was observed with DiI; smaller microbubbles (<20 μm) had an intensity per pixel of 5846 ± 1908 AU/pixel whereas microbubbles larger than 20 μm had an intensity per pixel of 1546 ± 58 AU/pixel (SI Table 1). These observations are again consistent with the exclusion of PEG-40-stearate from smaller bubbles.

A further aim of these experiments was to determine whether the presence of the emulsifier gave rise to domain formation on the surface of microbubbles within the clinical size range. It was intended that the fluorescent PEG-40-stearate analogue would provide a more direct means of determining emulsifier content and bubble coating structure compared with lipid analogue dyes. No domains were observed on microbubbles with diameters smaller than 5 μm. The DiI images indicated that some microbubbles with diameters between 5 and 20 μm did exhibit surface domains (Figure 5 K), similar to those reported previously [11]. The absence of a FITC signal in Panel J however indicates that the formation of domains was not necessarily associated with PEG-40-stearate[1]. This was further

[1] It also supports the implicit assumption that there was no energy transfer between the two dyes in the membrane i.e. from FITC-PEG40-sterate to DiI

suggested by the fact that there was limited overlap in the apparent domains visible in the DiI and FITC images (Figure 5 G, H and I).

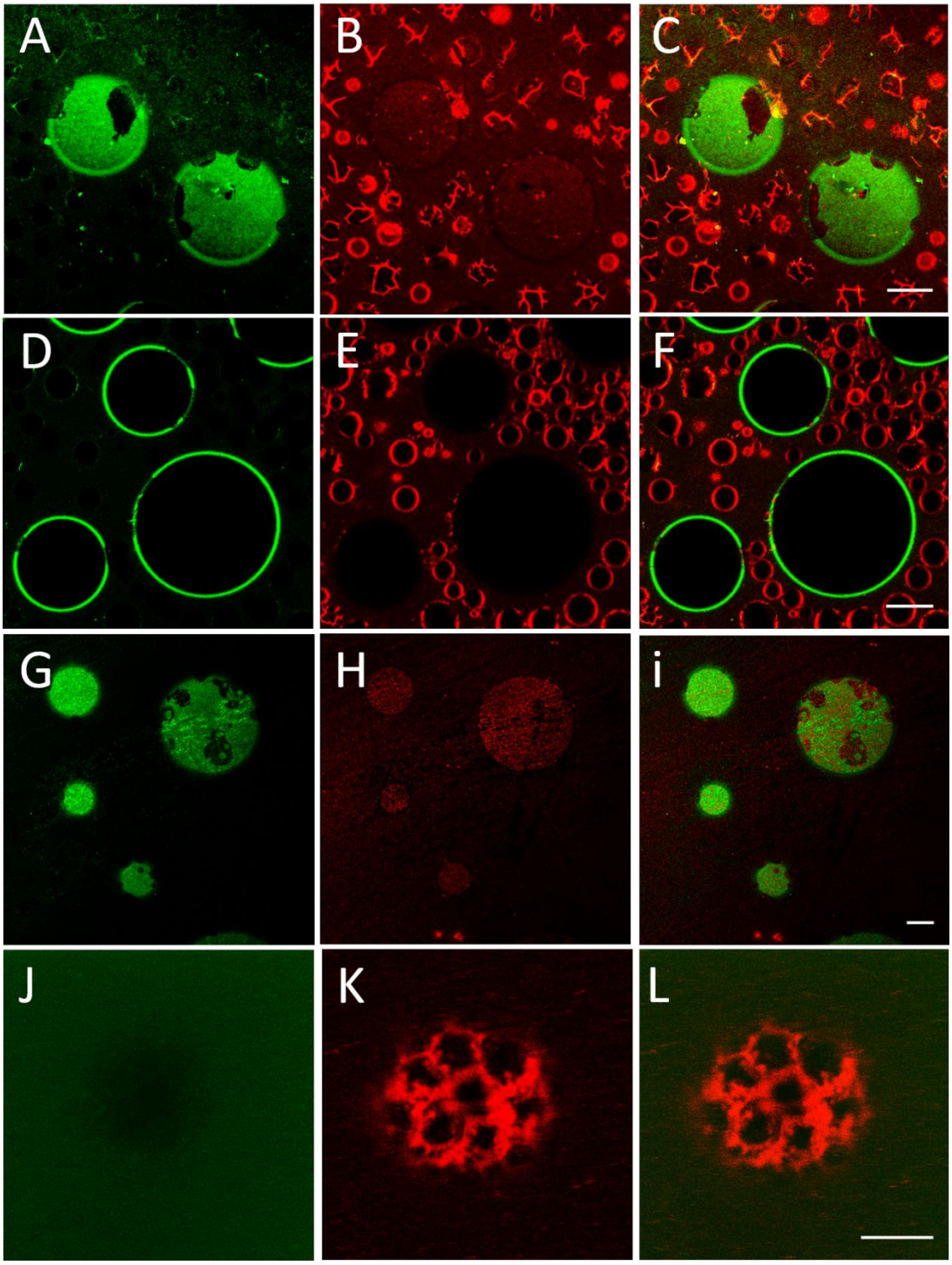

Figure 5, images of FITC-PEG-40-stearate and DiI stained microbubbles, unwashed. 1st column: FITC image, 2nd column: DiI, 3rd column: composite. Panels A, B and C show two microbubbles >20 µm surrounded by smaller microbubbles with the pinhole adjusted to emphasise phase separated regions. Panels D, E and F show the midplanes of microbubbles with diameters from 5 µm to 60 µm with the pinhole set to 1 airy unit. Panels G, H and I show microbubbles with diameters from 20 µm to 60 µm incorporating large quantities of FITC- PEG-40-stearate. G and H both appear to show domain formation but I shows that the separated regions do not overlap. Panels J, K and L show an 11 µm

diameter microbubble with domains clearly visible in the DiI image but a negligible FITC signal also suggesting that PEG-40-stearate was not present in the domains. Scale bars: C = 20 µm, F = 20 µm, I = 20 µm, L = 5 µm.

Examining PEG-40-stearate content within microbubbles

To investigate further whether PEG-40-stearate was excluded from microbubbles smaller than 5 µm in diameter, the microbubbles were centrifuged to remove any unincorporated PEG-40-stearate from the surrounding solution. Figure 6 A, B and C indicate that the FITC-PEG-40-stearate was in fact still present in microbubbles after centrifugation. The greyscale intensity profile across the microbubble surface indicates the increase in fluorescence corresponding to the microbubble coating (Figure 6C). This was observed for all microbubbles regardless of size (1 – 10 µm). Again, although there were variations in intensity across the microbubble coating, no domain like features were visible on microbubbles smaller than 5 µm in diameter. This suggests that PEG-40-stearate was uniformly distributed throughout the microbubble coating and not entirely excluded by surface pressure. ,

Microbubbles were also created with fluorescent PEG-40 alone, without stearic acid, as a negative control. In this case the fluorescent PEG-40 was found in solution and not in the microbubbles (Figure 6 D and E), as observed for the second greyscale values (Figure 6 F) after centrifugation. This suggests that PEG-40 does not passively attach to the microbubble surface and requires the stearic chain for incorporation into the microbubble coating.

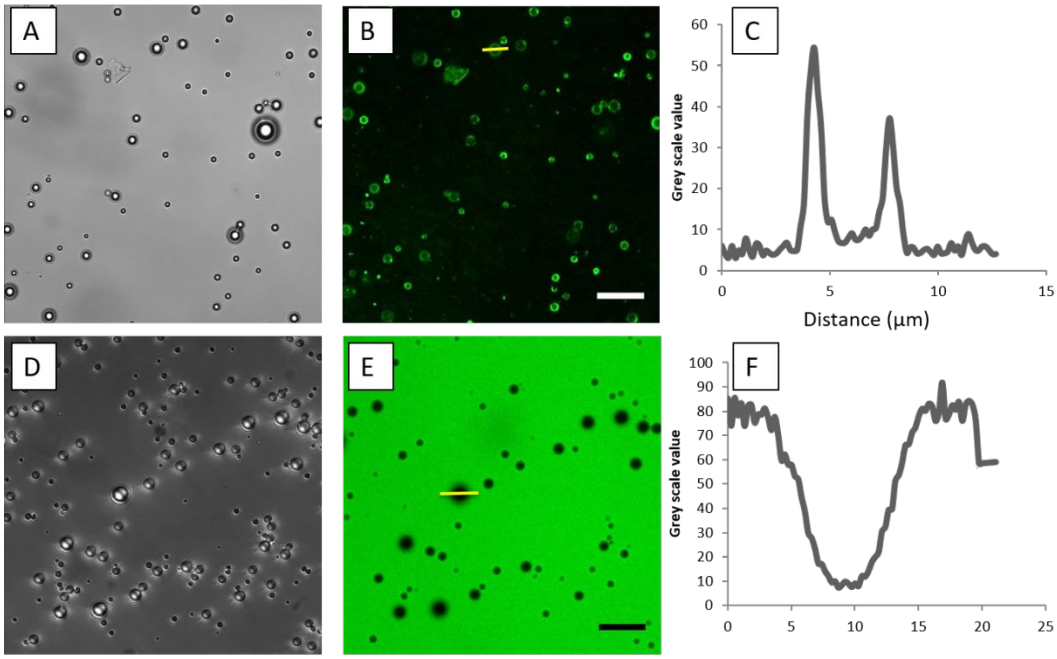

Figure 6 Fluorescent microbubbles. Centrifuged microbubbles created with a fluorescent PEG-40-stearate analogue in A) brightfield and B) fluorescence. C) Greyscale image of fluorescence intensity drawn across a microbubble (yellow line in B). D) Brightfield and E) fluorescent image of microbubbles created with fluorescent PEG-40 with no attached stearic acid. F) Greyscale image of highest fluorescence drawn across a microbubble (yellow line in E). (Scale bar 20 µm).

Comparison of microbubble size and concentration

Centrifugation of microbubbles

DSPC only microbubbles, DSPC:DSPE-PEG(2000) (9:1) and DSPC:PEG-40-Stearate (9:1) were formulated in triplicate in PBS. These were analysed for size and concentration, followed by centrifugation (1000 RPM, 10 min) whereby the supernatant and infranatant were also analysed. Centrifugation has been used to clean microbubbles and size isolate certain populations[28] and microbubble survival from centrifugation would provide information on stability. Results indicated that average size did not vary between microbubble samples within significance. However, after centrifugation the DSPC only microbubbles were more polydisperse relative to microbubbles formulated with DSPE-PEG(2000) and PEG-40 stearate (Figure 7A and B). The highest concentrations (Figure 7C) of

microbubbles were achieved with PEG-40 stearate (1 x 10^{11} microbubbles/ml), followed by DSPE-PEG(2000) (1 x 10^{10} microbubbles/ml), and finally DSPC alone (1 x 10^{9} microbubbles/ml). DSPE-PEG(2000) microbubbles were more stable to centrifugation maintaining the same average concentration as before centrifugation within experimental error, whereas PEG-40-Stearate microbubbles were lower in concentration (1 x 10^{9} microbubbles/ml) after centrifugation indicating microbubbles might be destroyed during the centrifugation process as shown in Figure 7 D. The data agrees with results from Lozano *et al.* on the condensed phase of the lipids resulting in increased stability when formulated with DSPE-PEG(2000)[11].

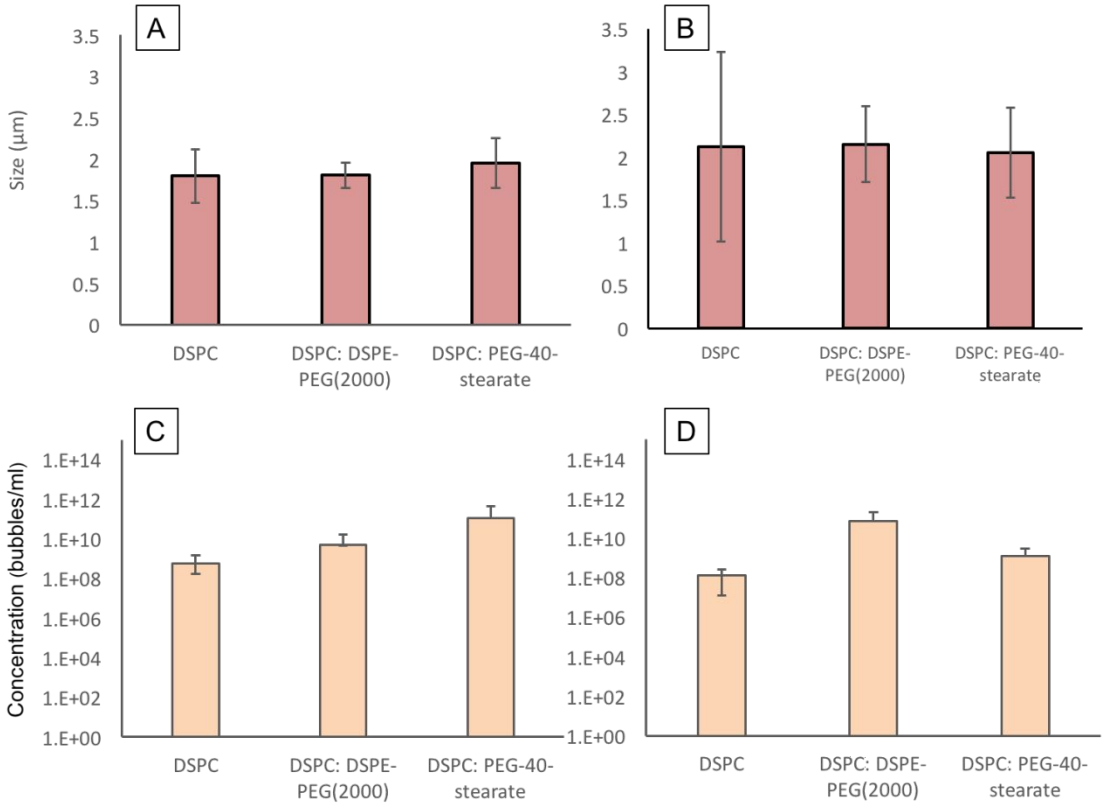

Figure 7 average diameter and average concentration of DSPC only microbubbles, DSPC:DSPE-PEG(2000) (9:1) and DSPC:PEG-40-Stearate (9:1). A) Size before centrifugation and B) after centrifugation. C) Concentration before centrifugation and D) after centrifugation. N = 3.

Size of vesicles

Vesicles present in the microbubble suspension were analysed by Dynamic Light Scattering, by taking a fluid sample just before sonicating at the gas/water interface. The results shown in Figure 8 indicate that DSPC and PEG-40-stearate produces vesicles (mean diameter: 117nm) in a smaller size range than DSPC alone (mean diameter: 1500nm). DSPC and DSPE-PEG(2000) also produces smaller vesicles as well (mean diameter: 105nm). This was as expected from previous literature [31]. The production of smaller vesicles could assist in the generation of the microbubble coating and the stability of the microbubble, according to the mechanism postulated by Li and Fogler [32] whereby vesicles break up through sonication at the gas water interface and fuse to form the microbubble coating. Hence the size of the vesicles plays an important role as smaller vesicles will have a higher surface energy, making microbubble formation more energetically favourable. These results are also consistent with observations of phospholipid coated microbubbles via electron microscopy by Owen *et al*., which also indicated that the coating comprised small vesicles [29]. The larger size of DSPC only vesicles might indicate that microbubbles generated from lipid fragments alone are less stable and in lower concentration whereas microbubbles incorporating a PEG moiety contain intact vesicles which have an impact on microbubble shell properties.

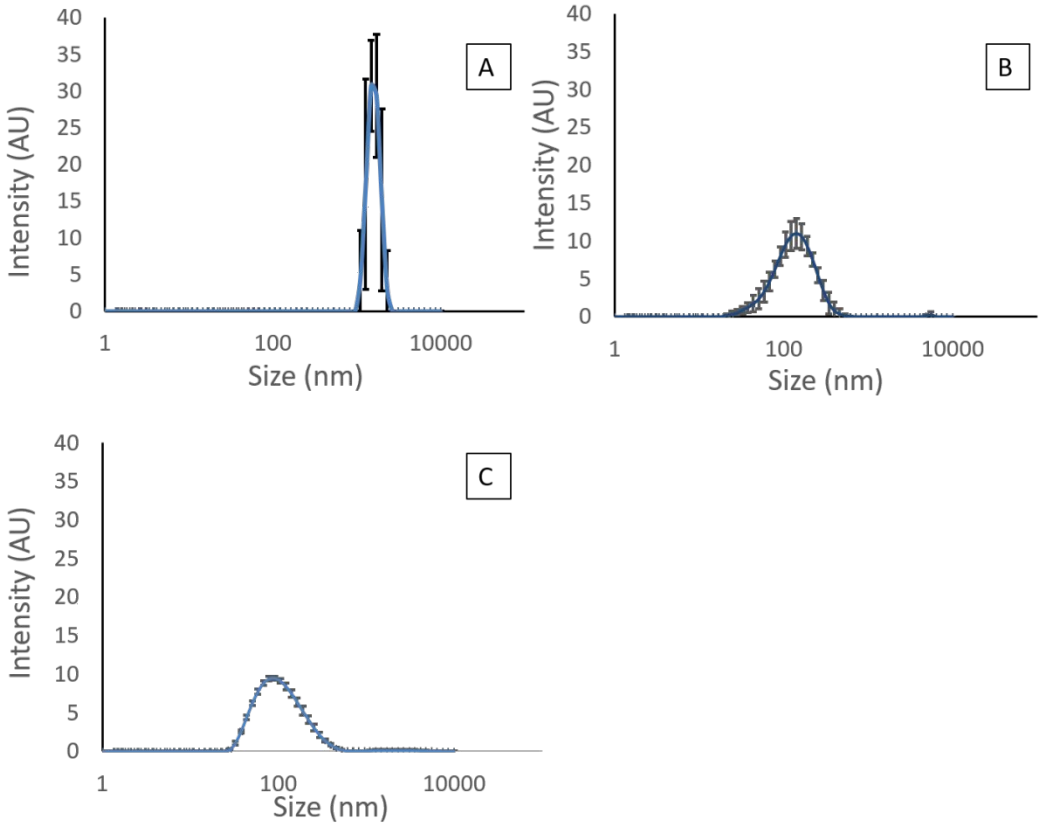

Figure 8 Dynamic light scattering results of vesicle solutions. A) DSPC alone and B) DSPC with PEG-40-stearate, C) DSPC with DSPE-PEG(2000). (n = 3).

The role of vesicles not incorporated into the microbubble coating requires further investigation. A recent study by Fix *et al.* examined the clearance of PEG coated microbubbles by anti-PEG antibodies showing that microbubbles incorporating DSPE-PEG were cleared faster over time after repeated administrations by anti-PEG antibodies[33]. The nanoscale vesicles present in the bubble population likely contain PEG and could have an impact on this effect.

Microbubble Serum Stability Study

DSPC:PEG-40-Stearate microbubbles and DSPC: DSPE-PEG(2000) microbubbles were prepared and added to human serum. At set time points, the microbubble concentration was analysed by Accusizer. Results indicate that over the course of

15 minutes at ambient temperature, the DSPE-PEG(2000) microbubbles remained at a higher concentration than the PEG-40-stearate microbubbles (Figure 9 A). This agrees with the work of Lozano *et al[11].* However, over the course of 10 minutes the difference in residual microbubble concentration is not statistically significant and microbubbles incorporating DSPE-PEG(2000) only showing a marked improvement at the 15 minute timepoint. Microbubble size and concentration were also measured over a period of 7 days from samples stored at 4^{o}C in a sealed vial (supplementary data) and showed similar trends. However, at 37 °C no difference between DSPE-PEG(2000) microbubbles and those formulated with PEG-40-stearate was observed at any time point. These differences in stability at different temperatures can be explained by comparing the isotherms of the two formulations. The isotherms for PEG-40-S containing monolayers show no significant change in form including the slope of the curves at all points and the pressure where the plateau appears, except that the size of the plateau shrinks. There exists a direct correspondence between the monolayer and bilayer surface pressure, and under equilibrium the two are equal [30-32]. Whilst the surface pressure for a bubble cannot be ascertained without a direct measurement, it can still be deduced from the isotherms that the compressibility of the film remains similar for all pressures when increasing the temperature from 18 to 37°C. In contrast, DSPE-PEG2000 containing films become more compressible with increasing temperature [33]. Statistical thermodynamics provide a direct relationship between lipid film permeability and its compressibility [34, 35] and thus the gas permeability of PEG40S bubble is expected to remain same while it is expected to increase for DSPE-PEG2000

bubbles bubble as the temperature is increased from 18 to 37°C, leading to a reduction in microbubble stability.

It is important to note, however, that "stability" in the context of clinical applications is also determined by lung and liver capture and further work is required to compare the *in vivo* circulatory stability of the two formulations.

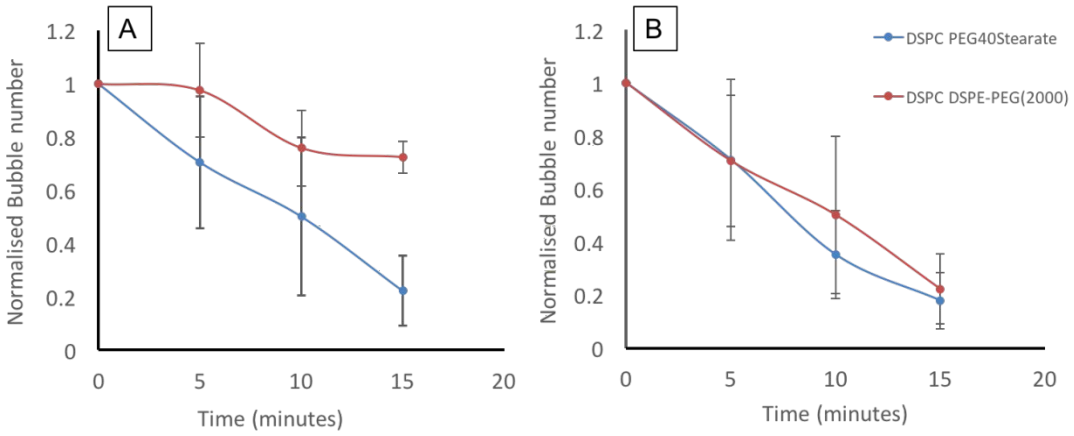

Figure 9 Serum stability of 9:1 DSPC microbubbles with PEG-40-Stearate and 9:1 DSPC microbubbles with DSPE-PEG(2000). A) Bubble concentration over 15 minutes in human serum at room temperature, B) Bubble concentration over 15 minutes in human serum at 37 ˚C (n=3).

Backscatter acoustic intensity comparison of microbubbles

The average backscatter intensity of 9:1 DSPC microbubbles with PEG-40-Stearate and 9:1 DSPC microbubbles with DSPE-PEG(2000) was compared as shown in Figure 10. No significant difference was seen between the two microbubble formulations ($p = 0.3719$), indicating that both types of bubble would behave similarly as ultrasound contrast agents.

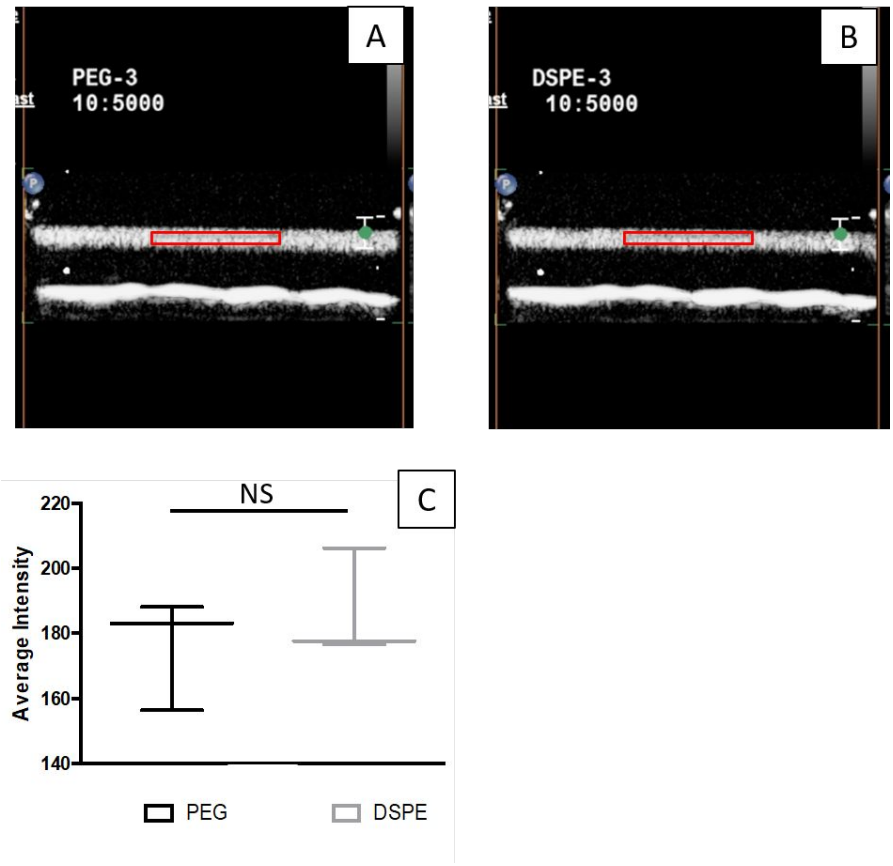

Figure 10, Acoustic intensity of 9:1 DSPC microbubbles with PEG-40-Stearate and 9:1 DSPC microbubbles with DSPE-PEG(2000). A) Representative (contrast mode) image of 9:1 DSPC microbubbles with PEG-40-Stearate in the flow phantom and B) Representative (contrast mode) image of 9:1 DSPC microbubbles with DSPE-PEG(2000) in the flow phantom. Red box is the region of interest used to quantify the backscatter intensity for each image. C) Average intensity of two microbubble populations. Significance was measured using a student's one tailed t-test (n=3).

CONCLUSIONS

A fluorescent form of PEG-40-stearate was successfully synthesised and used to determine the location of the PEG-40-stearate molecule within a lipid microbubble coating. Langmuir trough measurements revealed that PEG-40-stearate changes the isotherm of DSPC alone and images of the fluorescent PEG-40-stearate analogue indicated domain formation and vesicles entering the solution and leaving the lipid film at 30 mN/m in contrast to films of DSPE-PEG(2000) and DSPC alone in which coating integrity was maintained.

Spectral imaging showed that PEG-40-stearate did not have a statistically significant impact on lipid order in the bubble coating at any concentration. This indicates that PEG-40-stearate likely enhances microbubble formation without impacting shell properties and that most PEG-40-stearate is excluded from the coating and enters the solution. Fluorescence microscopy, however, revealed that some PEG-40-stearate does remain within the bubble coating.

Staining with DiI allowed observation of domains as previously reported by Borden *et al* [9]. In the present study, however, domains were also only observed on larger microbubbles (> 5 μm). In addition, the proportion PEG-40-stearate was higher in microbubbles with diameters >8 μm.

No differences in microbubble size or concentration were found relative to DSPE-PEG(2000) formulated microbubbles and both PEG-40-stearate and DSPE-PEG(2000) were stable to centrifugation. Both formulations created ~100 nm vesicles indicating similar microbubble formation mechanisms.

At room temperature DSPE-PEG(2000) microbubbles maintained a higher concentration for a longer period of time in human serum than PEG-40-stearate microbubbles. However, at 37 °C no statistically significant difference could be discerned. Furthermore no statistical difference was found in acoustic intensity between the two microbubble populations in a flow phantom at 37 °C.

Acknowledgements

The Authors thank the Engineering and Physical Sciences Research Council for funding the work through grants EP/I021795/1 and EP/L024012/1. E. Stride thanks the Institute of Engineering and Technology for support through the AF Harvey prize. J. F. Callan thanks Norbrook Laboratories Ltd. for funding an endowed chair.

References

1. Quaia, E., *Contrast Media in Ultrasonography*. 2005.
2. Stride, E. and M. Edirisinghe, *Novel microbubble preparation technologies.* Soft Matter, 2008. **4**(12): p. 2350.
3. !!! INVALID CITATION !!! [3-5].
4. McEwan, C., et al., *Oxygen carrying microbubbles for enhanced sonodynamic therapy of hypoxic tumours.* Journal of Controlled Release, 2015. **203**: p. 51-56.
5. Owen, J., et al., *Reducing tumour hypoxia via oral administration of oxygen nanobubbles.* PLoS ONE, 2016. **11**(12).
6. Spahn, D.R., *Blood substitutes.* Critical Care, 1999. **3**(5): p. R91-R92.
7. Ferrara, K.W., M.A. Borden, and H. Zhang, *Lipid-Shelled Vehicles: Engineering for Ultrasound Molecular Imaging and Drug Delivery.* Accounts of Chemical Research, 2009. **42**(7): p. 881-892.
8. Kim, D.H., et al., *Mechanical properties and microstructure of polycrystalline phospholipid monolayer shells: Novel solid microparticles.* Langmuir, 2003. **19**(20): p. 8455-8466.
9. Borden, M.A., et al., *Surface phase behavior and microstructure of lipid/PEG-emulsifier monolayer-coated microbubbles.* Colloids and Surfaces B: Biointerfaces, 2004. **35**(3-4): p. 209-223.
10. Borden, M.A., et al., *Lateral phase separation in lipid-coated microbubbles.* Langmuir, 2006. **22**(9): p. 4291-4297.
11. Lozano, M.M. and M.L. Longo, *Microbubbles Coated with Disaturated Lipids and DSPE-PEG2000: Phase Behavior, Collapse Transitions, and Permeability.* Langmuir, 2009. **25**(6): p. 3705-3712.
12. Gerber, F., et al., *Fluidization of a dipalmitoyl phosphatidylcholine monolayer by fluorocarbon gases: Potential use in lung surfactant therapy.* Biophysical Journal, 2006. **90**(9): p. 3184-3192.
13. Venegas, B., et al., *High Vapor Pressure Perfluorocarbons Cause Vesicle Fusion and Changes in Membrane Packing.* Biophysical Journal, 2008. **95**(10): p. 4737-4747.
14. Fainerman, V.B., E.V. Aksenenko, and R. Miller, *Influence of alkane and perfluorocarbon vapors on adsorbed surface layers and spread insoluble*

monolayers of surfactants, proteins and lipids. Advances in Colloid and Interface Science, 2017. **244**: p. 100-112.
15. Kooiman, K., et al., *DSPC or DPPC as main shell component influences ligand distribution and binding area of lipid-coated targeted microbubbles.* European Journal of Lipid Science and Technology, 2014.
16. Abou-Saleh, R.H., et al., *Poly(ethylene glycol) Lipid-Shelled Microbubbles: Abundance, Stability, and Mechanical Properties.* Langmuir, 2014. **30**(19): p. 5557-5563.
17. Shih, R. and A.P. Lee, *Post-Formation Shrinkage and Stabilization of Microfluidic Bubbles in Lipid Solution.* Langmuir, 2016. **32**(8): p. 1939-1946.
18. Segers, T., et al., *Stability of Monodisperse Phospholipid-Coated Microbubbles Formed by Flow-Focusing at High Production Rates.* Langmuir, 2016. **32**(16): p. 3937-3944.
19. Carugo, D., et al., *Modulation of the molecular arrangement in artificial and biological membranes by phospholipid-shelled microbubbles.* Biomaterials, 2017. **113**: p. 105-117.
20. Hosny, N.A., et al., *Mapping microbubble viscosity using fluorescence lifetime imaging of molecular rotors.* Proceedings of the National Academy of Sciences of the United States of America, 2013. **110**(23): p. 9225-9230.
21. Aron, M., et al., *Spectral imaging toolbox: Segmentation, hyperstack reconstruction, and batch processing of spectral images for the determination of cell and model membrane lipid order*. Vol. 18. 2017. 254.
22. Parasassi, T., et al., *Cholesterol modifies water concentration and dynamics in phospholipid bilayers: a fluorescence study using Laurdan probe.* Biophysical Journal, 1994. **66**(3, Part 1): p. 763-768.
23. Sennoga, C.A., et al., *On sizing and counting of microbubbles using optical microscopy.* Ultrasound in Medicine and Biology, 2010. **36**(12): p. 2093-2096.
24. Borden, M.A., et al., *Ultrasound radiation force modulates ligand availability on targeted contrast agents.* Molecular imaging : official journal of the Society for Molecular Imaging, 2006. **5**(3): p. 139-147.
25. Quaia, E., *Microbubble ultrasound contrast agents: An update.* European Radiology, 2007. **17**(8): p. 1995-2008.
26. Mannaris, C., et al., *Gas-Stabilizing Gold Nanocones for Acoustically Mediated Drug Delivery.* Advanced Healthcare Materials, 2018. **7**(12): p. 1800184.
27. Albrecht, O., H. Gruler, and E. Sackmann, *Polymorphism of phospholipid monolayers.* J. Phys. France, 1978. **39**(3): p. 301-313.
28. Feshitan, J.A., et al., *Microbubble size isolation by differential centrifugation.* Journal of Colloid and Interface Science, 2009. **329**(2): p. 316-324.
29. Owen, J. and E. Stride, *Technique for the Characterization of Phospholipid Microbubbles Coatings by Transmission Electron Microscopy.* Ultrasound in Medicine and Biology, 2015. **41**(12): p. 3253-3258.
30. Feng, S.-s., *Interpretation of Mechanochemical Properties of Lipid Bilayer Vesicles from the Equation of State or Pressure–Area Measurement of the Monolayer at the Air–Water or Oil–Water Interface.* Langmuir, 1999. **15**(4): p. 998-1010.
31. Jähnig, F., *What is the surface tension of a lipid bilayer membrane?* Biophysical Journal, 1996. **71**(3): p. 1348-1349.

32. MacDonald, R.C. and S.A. Simon, *Lipid monolayer states and their relationships to bilayers.* Proceedings of the National Academy of Sciences, 1987. **84**(12): p. 4089-4093.
33. Chou, T.-H. and I.M. Chu, *Thermodynamic characteristics of DSPC/DSPE-PEG2000 mixed monolayers on the water subphase at different temperatures.* Colloids and Surfaces B: Biointerfaces, 2003. **27**(4): p. 333-344.
34. Nagle, J.F. and H.L. Scott, *Lateral compressibility of lipid mono- and bilayers. Theory of membrane permeability.* Biochimica et Biophysica Acta (BBA) - Biomembranes, 1978. **513**(2): p. 236-243.
35. Wunderlich, B., et al., *Phase-State Dependent Current Fluctuations in Pure Lipid Membranes.* Biophysical Journal, 2009. **96**(11): p. 4592-4597.

Supplementary Information

Table S1, Intensity/pixel of FITC and DiI for microbubbles of different diameters.

Bubble diameter (μm)	pixels	intensity FITC	Intensity /pixel	Intensity DiI	Intensity DiI/pixel
40	15736	84531039	5371.825051	24286345	1543.362036
38	14642	83333739	5691.417771	21636047	1477.670195
62	25018	141342615	5649.636861	40493420	1618.571429
11	3509	9232503	2631.092334	18870682	5377.794813
10	2014	4861347	2413.777061	7611523	3779.306356
11	2036	5877110	2886.596267	17067897	8383.053536

Figure S2, Microbubble diameter as a function of time when stored in a sealed vial at 4°C.

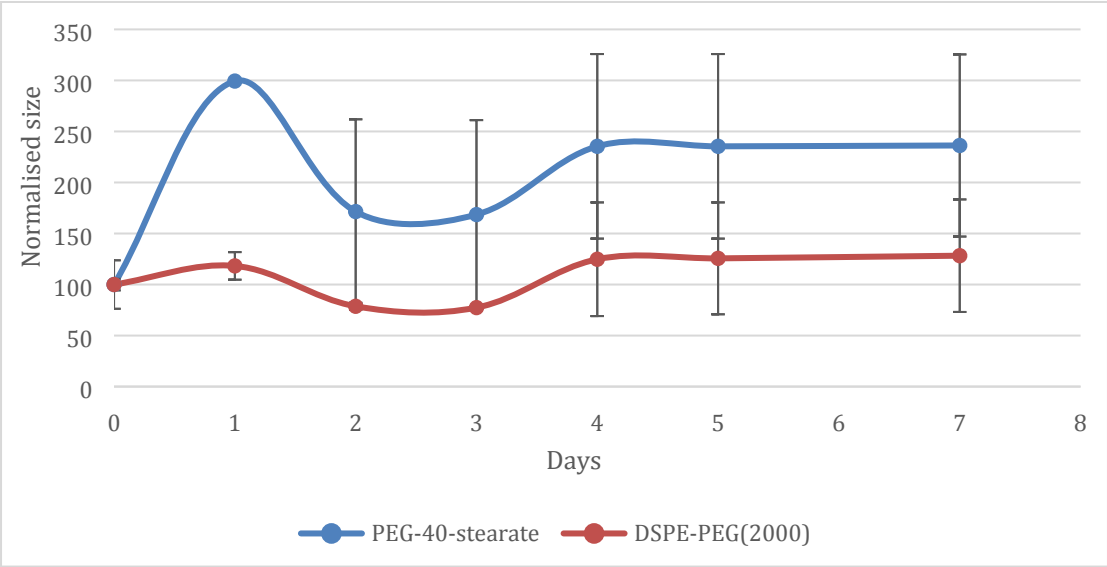

Figure S2, Microbubble concentration as a function of time when stored in a sealed vial at 4°C.

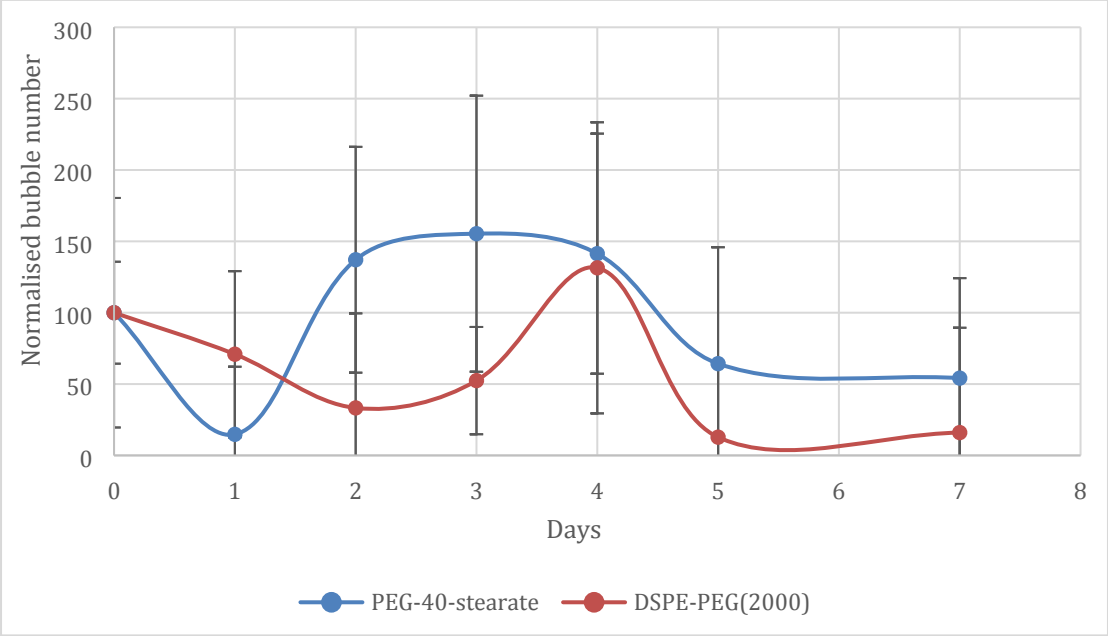

Table of Contents Graphic

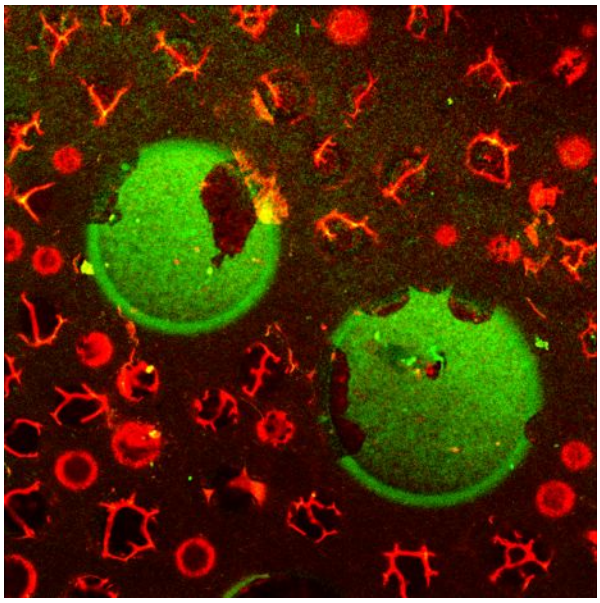

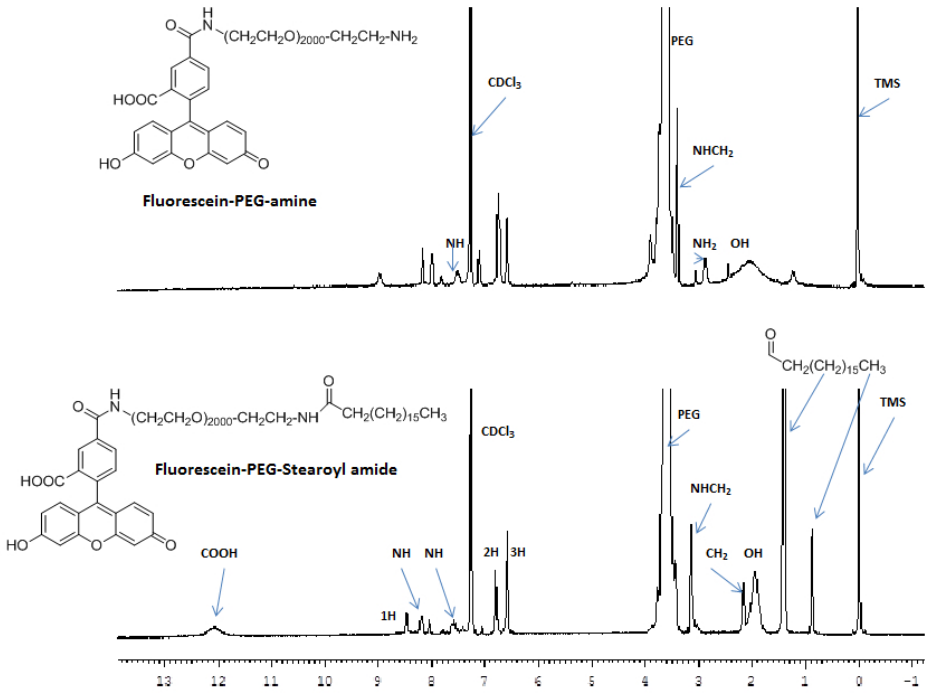

Figure 1, 1H NMR spectra of Fluorescein-PEG and Fluorescein-PEG- Stearate (Solvent: CDCl3).

236x173mm (96 x 96 DPI)

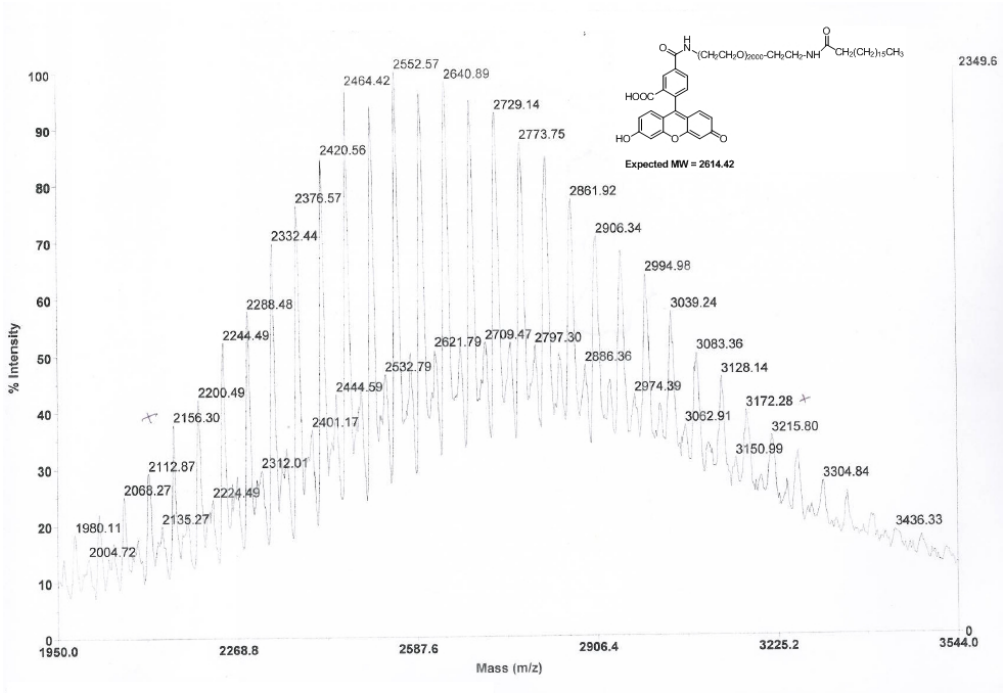

Figure 2, Maldi-TOF spectra of Fluorescein-PEG- Stearate amide indicating that stearic acid had been attached to the fluorescent PEG chain.

258x178mm (96 x 96 DPI)

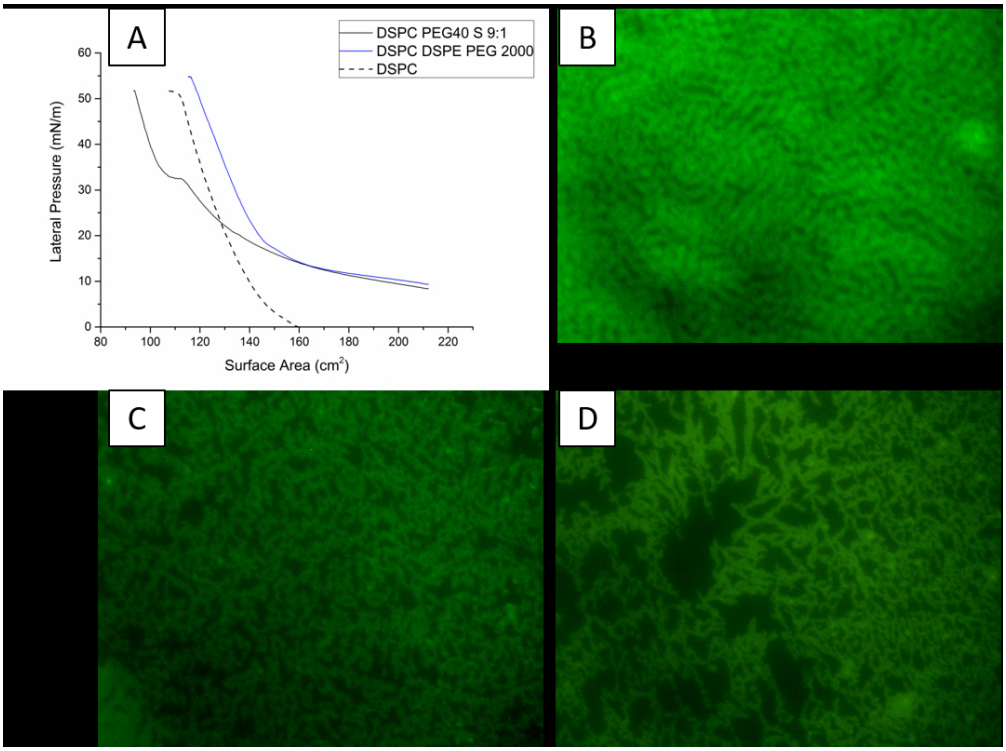

Figure 3, Langmuir trough measurements at A) Lateral pressure vs area isotherms of DSPC monolayer with and without modifications, B) low (~10mN/m), C) medium (~25mN/m) to D) high lateral pressure (~40mN/m) showing the formation of domains in a mixed film of fluorescent PEG-40-stearate in DSPC. Arrow indicates vesicle like structures.

182x135mm (150 x 150 DPI)

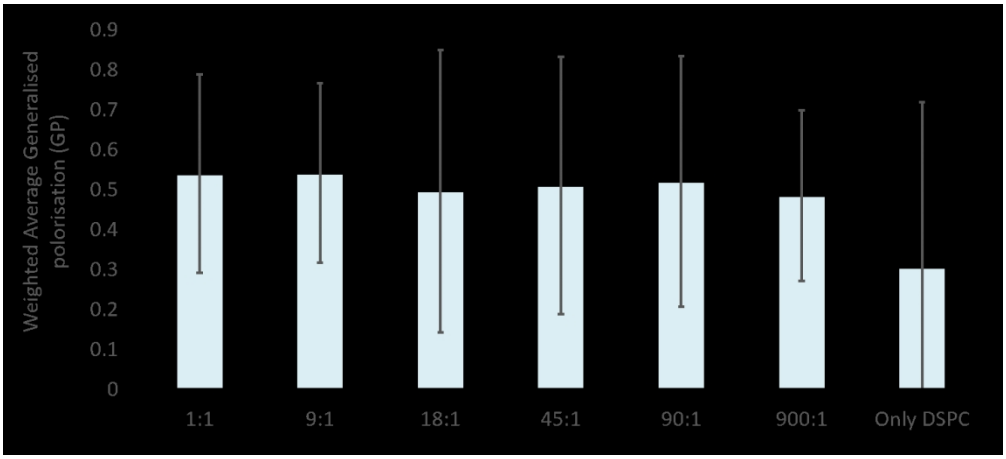

Figure 4, Weighted average generalised polarisation, at different ratios of DSPC to PEG-40-Stearate (n = 35)

249x112mm (150 x 150 DPI)

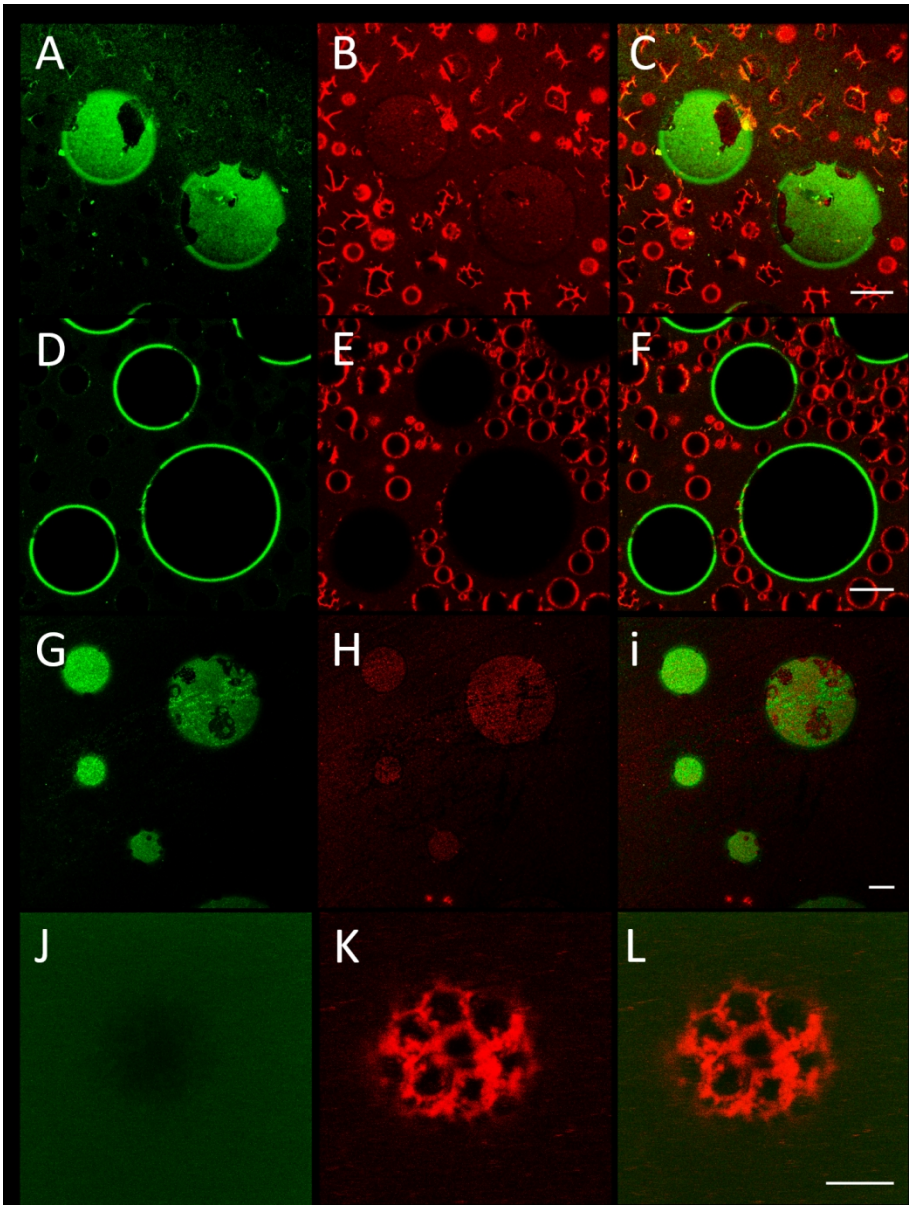

243x322mm (150 x 150 DPI)

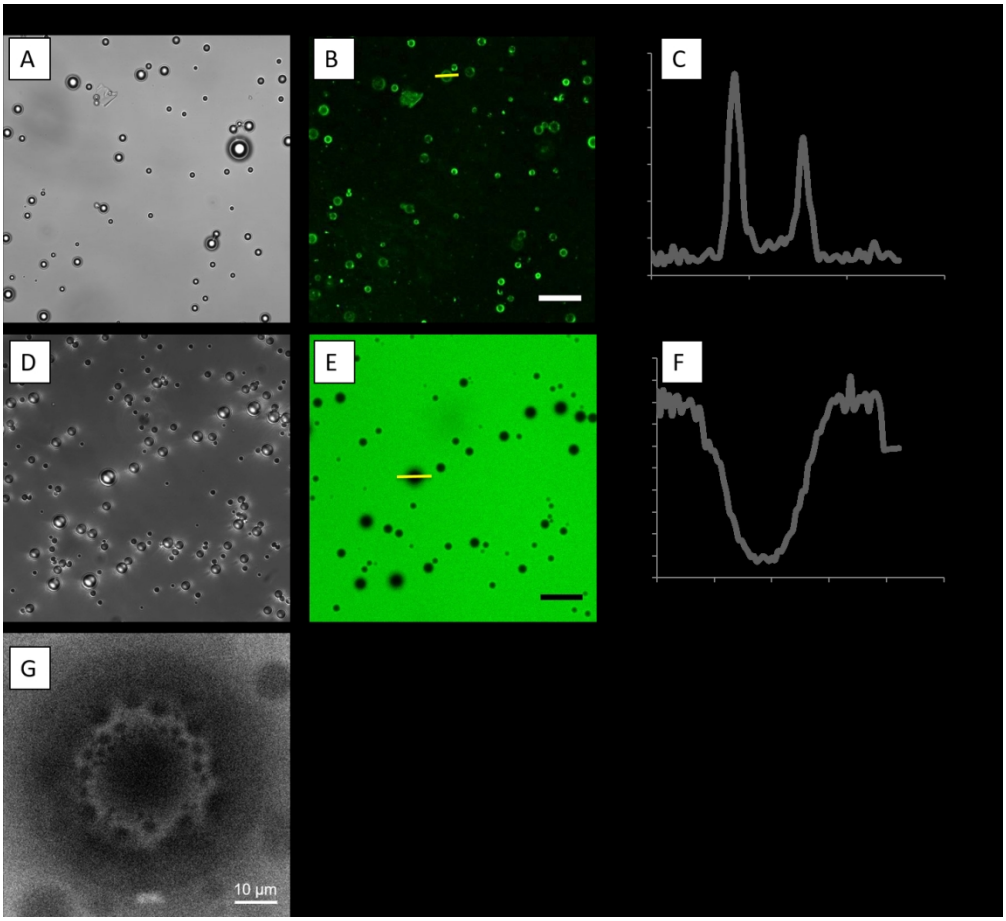

Figure 6 Fluorescent microbubbles. Centrifuged microbubbles created with fluorescent PEG-40-stearate in A) brightfield and B) fluorescence. C) Greyscale image of fluorescence intensity drawn across a microbubble (yellow line in B). D) Brightfield and E) fluorescent image of microbubbles created with fluorescent PEG-40 with no attached stearic acid. F) Greyscale image of highest fluorescence drawn across a microbubble (yellow line in E). (Scale bar 20 µm).

244x222mm (150 x 150 DPI)

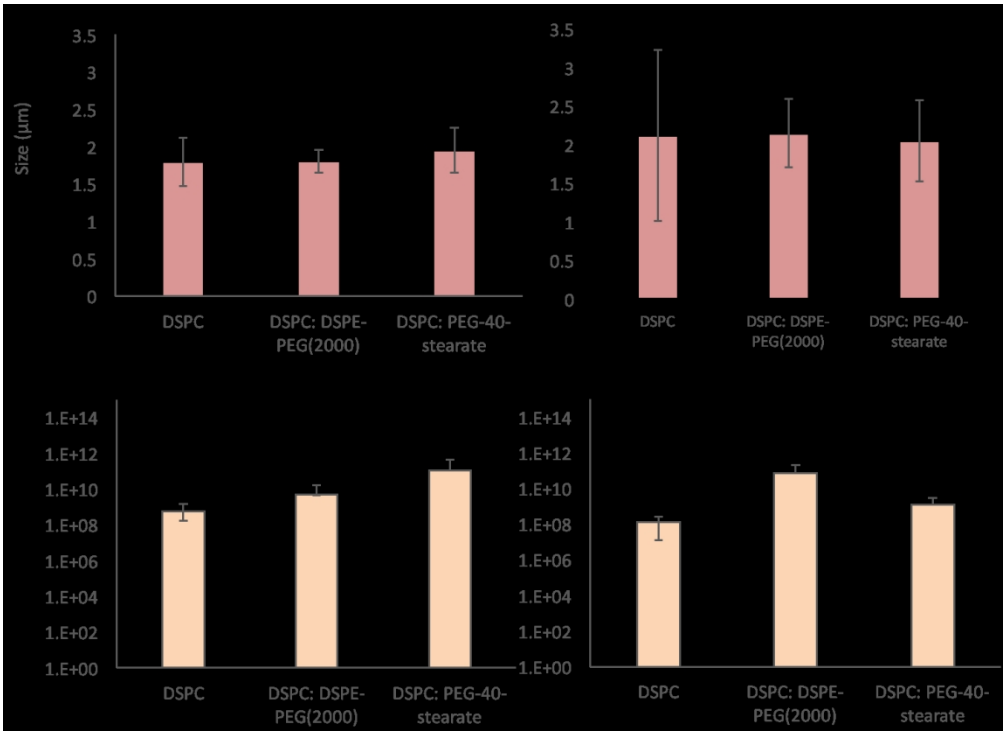

Figure 7 average diameter and average concentration of DSPC only microbubbles, DSPC:DSPE-PEG(2000) (9:1) and DSPC:PEG-40-Stearate (9:1). A) Size before centrifugation and B) after centrifugation. C) Concentration before centrifugation and D) after centrifugation. N = 3.

252x183mm (150 x 150 DPI)

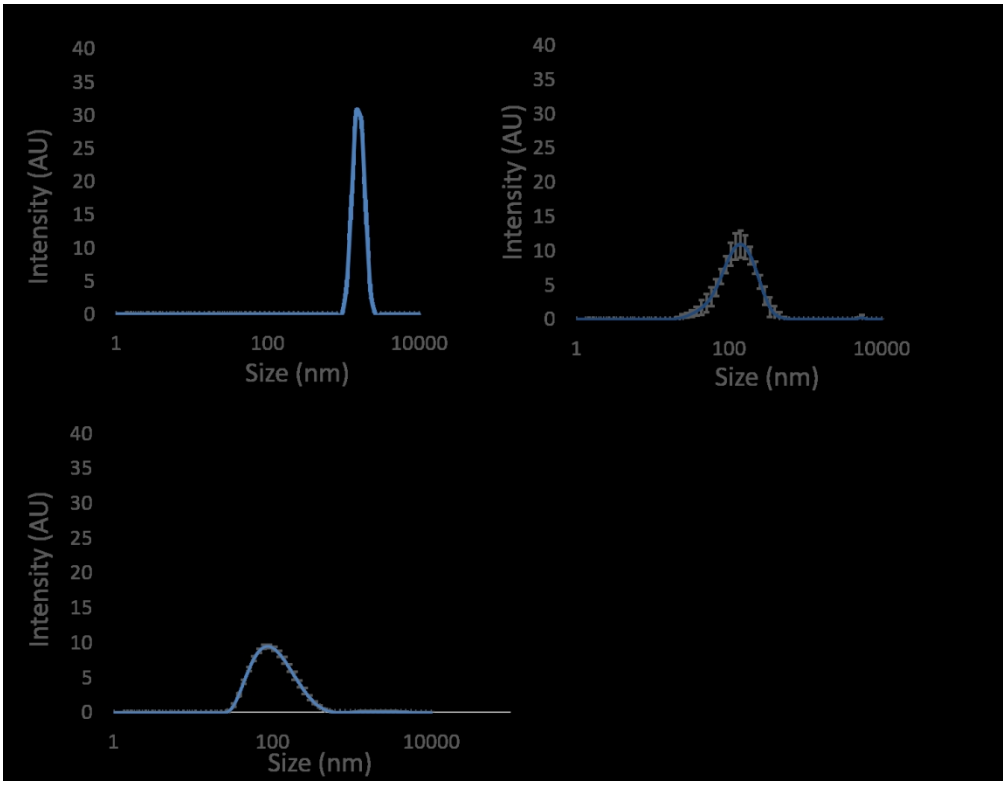

Figure 8 Dynamic light scattering results of vesicle solutions. A) DSPC alone and B) DSPC with PEG-40-stearate, C) DSPC with DSPE-PEG(2000). (n = 3).

251x195mm (150 x 150 DPI)

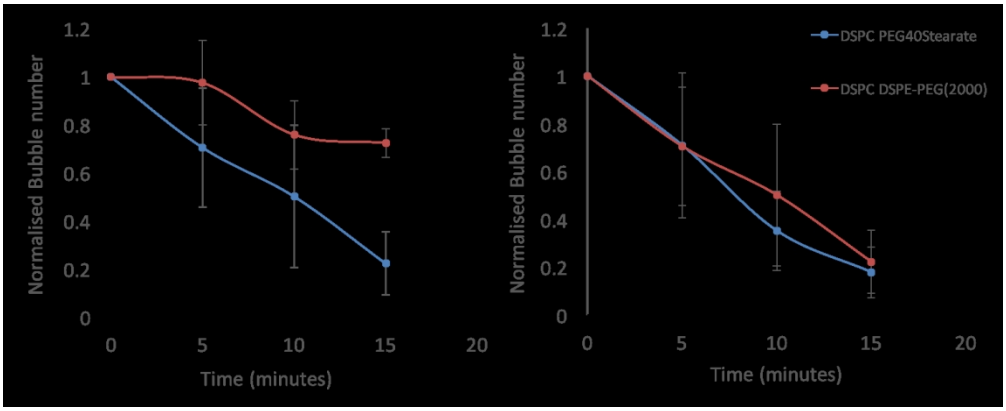

Figure 9 Serum stability of 9:1 DSPC microbubbles with PEG-40-Stearate and 9:1 DSPC microbubbles with DSPE-PEG(2000). A) Bubble concentration over 15 minutes in human serum at room temperature, B) Bubble concentration over 15 minutes in human serum at 37 °C (n=3).

260x104mm (150 x 150 DPI)

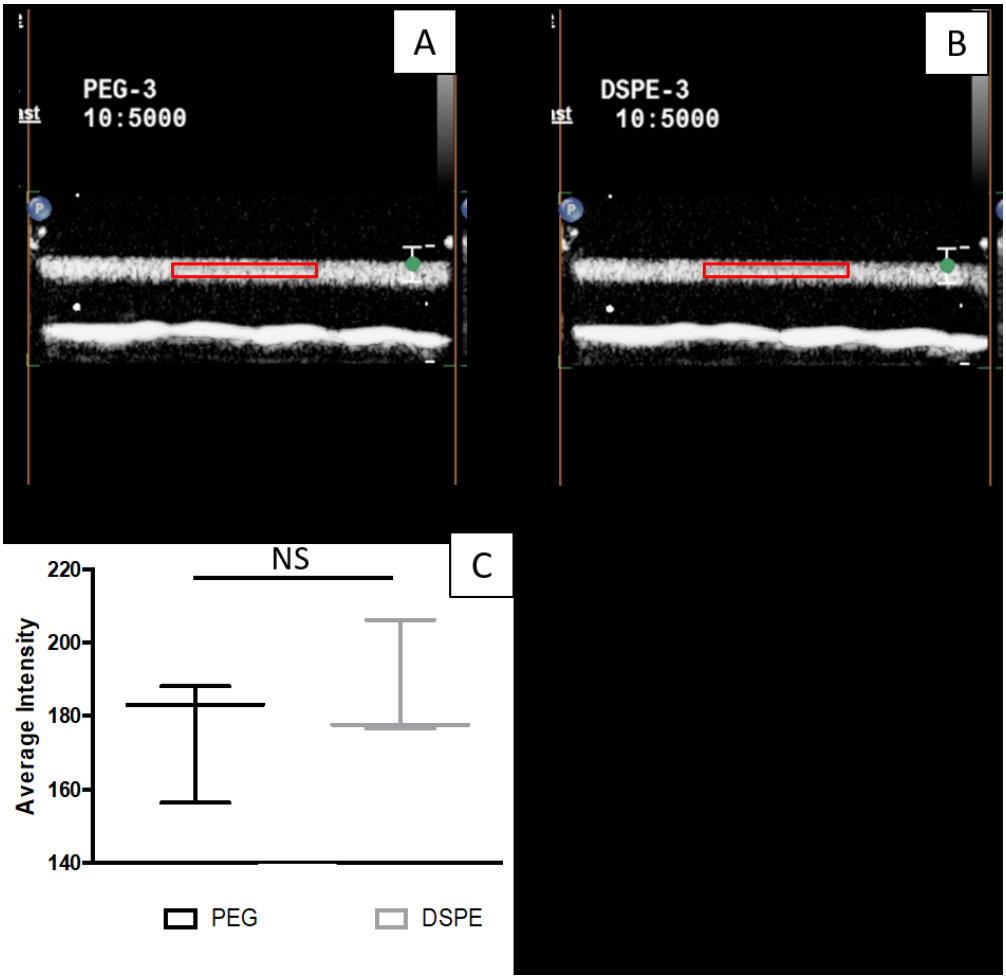

Figure 10, Acoustic intensity of 9:1 DSPC microbubbles with PEG-40-Stearate and 9:1 DSPC microbubbles with DSPE-PEG(2000). A) Representative (contrast mode) image of 9:1 DSPC microbubbles with PEG-40-Stearate in the flow phantom and B) Representative (contrast mode) image of 9:1 DSPC microbubbles with DSPE-PEG(2000) in the flow phantom. Red box is the region of interest used to quantify the backscatter intensity for each image. C) Average intensity of two microbubble populations. Significance was measured using a student's one tailed t-test (n=3).

160x155mm (150 x 150 DPI)

Scheme 1. Synthesis of Fluorescein-PEG- Stearate

90x50mm (192 x 192 DPI)

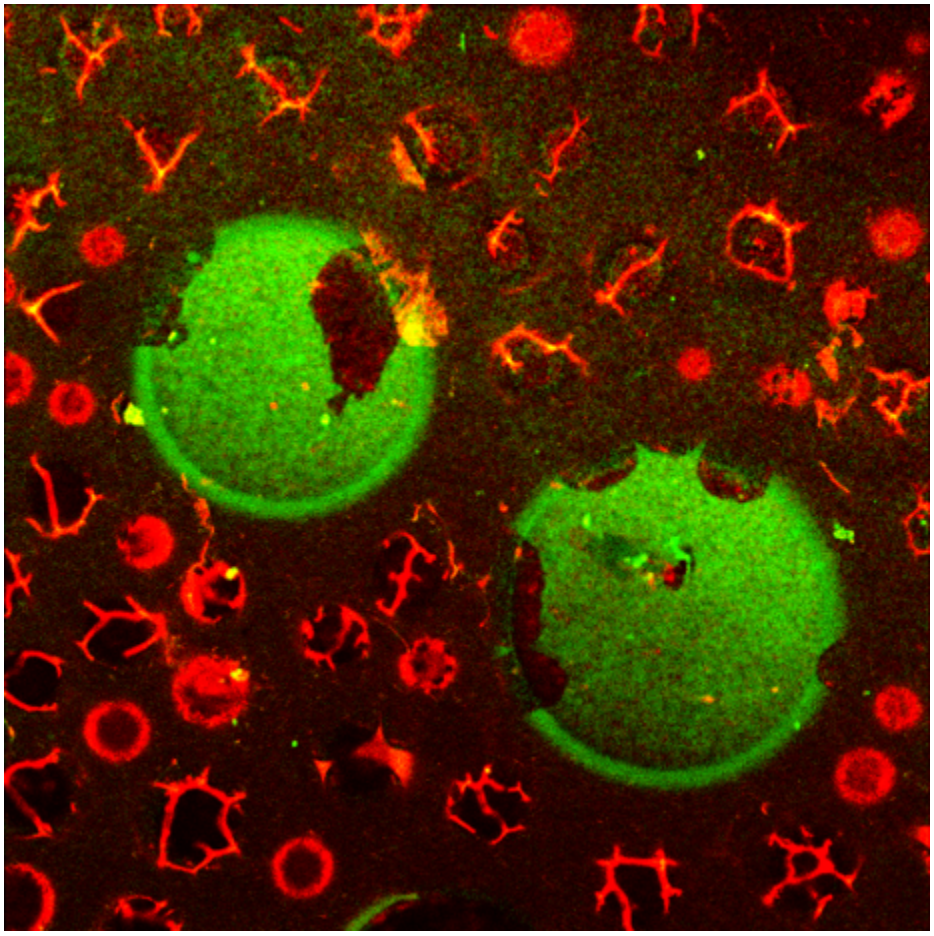

78x78mm (150 x 150 DPI)